

Graphical Abstract

Optimal-rate error estimates and a twice decoupled solver for a backward Euler finite element scheme of the Doyle-Fuller-Newman model of lithium-ion cells *

Shu Xu, Liqun Cao

Highlights

Optimal-rate error estimates and a twice decoupled solver for a backward Euler finite element scheme of the Doyle-Fuller-Newman model of lithium-ion cells

Shu Xu, Liquan Cao

- Comprehensive numerical analysis and implementation of the most widely used multiscale and multiphysics model for lithium-ion cells.
- Optimal-order error estimates in the norms $l^2(H^1)$ and $l^2(L^2(H_r^q))$, $q = 0, 1$, are rigorously established.
- Numerical convergence rates in both 2D and 3D are validated, which is inaccessible in the literature.
- A novel solver is designed to accelerate computation and reduce memory overhead, effectively handling strong nonlinearity and multiscale complexity.
- Three-dimensional numerical experiments with real battery parameters demonstrate that the proposed solver is the fastest and flexible to balance performance.

Optimal-rate error estimates and a twice decoupled solver for a backward Euler finite element scheme of the Doyle-Fuller-Newman model of lithium-ion cells

Shu Xu^{a,b,*}, Liqun Cao^{b,c,d}

^a*School of Mathematical Sciences, Peking University, Beijing, 100871, China*

^b*Institute of Computational Mathematics and Scientific/Engineering Computing,
Academy of Mathematics and Systems Science, Chinese Academy of
Sciences, Beijing, 100190, China*

^c*State Key Laboratory of Scientific and Engineering Computing, Beijing, 100190, China*

^d*National Center for Mathematics and Interdisciplinary Sciences, Chinese Academy of
Sciences, Beijing, 100190, China*

Abstract

We investigate the convergence of a backward Euler finite element discretization applied to a multi-domain and multi-scale elliptic-parabolic system, derived from the Doyle-Fuller-Newman model for lithium-ion cells. We establish optimal-order error estimates for the solution in the norms $l^2(H^1)$ and $l^2(L^2(H_r^q))$, $q = 0, 1$. To improve computational efficiency, we propose a novel solver that accelerates the solution process and controls memory usage. Numerical experiments with realistic battery parameters validate the theoretical error rates and demonstrate the significantly superior performance of the proposed solver over existing solvers.

Keywords: Elliptic-parabolic system, Lithium-ion cells, DFN model, Finite element, Error analysis, Multiscale and multiphysics model

2020 MSC: 65M15, 65M60, 65N15, 65N30, 78A57

*This work was funded by the National Natural Science Foundation of China (grant 12371437) and the Beijing Natural Science Foundation (grant Z240001).

*Corresponding author

Email addresses: xushu@lsec.cc.ac.cn (Shu Xu), clq@lsec.cc.ac.cn (Liqun Cao)

1. Introduction

The Doyle-Fuller-Newman (DFN) model [1, 2], commonly referred to as the pseudo-two-dimensional (P2D) model when the cell region is simplified to one dimension, is the most widely used physics-based model for lithium-ion cells. It is essential in various engineering applications, including estimating the state of charge (SOC), analyzing capacity performance under diverse operating conditions, and generating impedance spectra [3, 4, 5, 6, 7, 8]. Furthermore, as a cornerstone of battery modeling, it provides a foundation for incorporating additional physics, such as temperature effects and mechanical stress, enabling various model extensions [9, 10, 11, 12].

In this paper, we examine the following fully coupled nonlinear elliptic-parabolic system that characterizes the DFN model:

$$\begin{cases} -\nabla \cdot (\kappa_1 \nabla \phi_1 - \kappa_2 \nabla f(c_1)) = a_2 J, & (x, t) \in \Omega_1 \times (0, T), \\ -\nabla \cdot (\sigma \nabla \phi_2) = -a_2 J, & (x, t) \in \Omega_2 \times (0, T), \\ \varepsilon_1 \frac{\partial c_1}{\partial t} - \nabla \cdot (k_1 \nabla c_1) = a_1 J, & (x, t) \in \Omega_1 \times (0, T), \\ \frac{\partial c_2}{\partial t} - \frac{1}{r^2} \frac{\partial}{\partial r} (r^2 k_2 \frac{\partial c_2}{\partial r}) = 0, & (x, r, t) \in \Omega_{2r} \times (0, T), \end{cases} \quad (1)$$

where $\Omega_2 \subset \Omega_1 \subset \mathbb{R}^N$ and $\Omega_{2r} \subset \mathbb{R}^N \times \mathbb{R}_+$, $N = 1, 2, 3$, represent multiply connected domains. It is notable that the last equation does not involve x -differential operators, and Ω_{2r} spans two distinct scales x and r . Specifically, for each point $x \in \Omega_2$, there exists a singular parabolic equation defined over the r -coordinate.

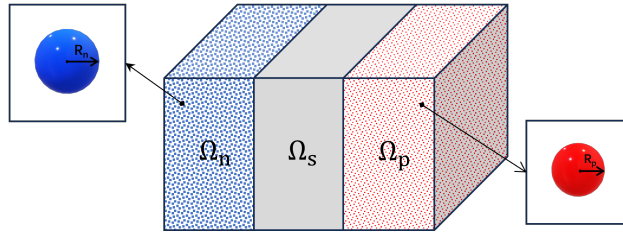


Figure 1: A 3D schematic representation of a Li-ion cell.

In the DFN model, a lithium-ion cell occupies a domain $\Omega \subset \mathbb{R}^N$, where $1 \leq N \leq 3$, comprising three subdomains: the positive electrode Ω_p , the negative electrode Ω_n , and the separator Ω_s . These regions typically form a laminated box structure, with $\Omega = \Omega_n \cup \Omega_s \cup \Omega_p$, as illustrated in Figure 1. Following a macrohomogeneous approach, it is assumed that the electrode

and electrolyte phases coexist within Ω_2 , and spherical particles with radii R_p and R_n are uniformly distributed throughout the electrodes, parameterized by the coordinates $(x, r) \in \Omega_{2r} := (\Omega_n \times (0, R_n)) \cup (\Omega_p \times (0, R_p))$. We define the electrolyte region as $\Omega_1 = \Omega_n \cup \Omega_s \cup \Omega_p$ and the electrode region as $\Omega_2 = \Omega_n \cup \Omega_p$. The model seeks to solve for four key variables: the electrolyte potential $\phi_1(x, t)$, the electrode potential $\phi_2(x, t)$, the lithium-ion concentration in the electrolyte $c_1(x, t)$, and the lithium concentration within the particles $c_2(x, r, t)$.

The multi-domain characteristics of the DFN model imply that the coefficients and nonlinear functions exhibit discontinuities across subdomains. Let $\mathbf{1}_{\Omega_m}$ denote the indicator function for the subdomain Ω_m . It is assumed that ε_1 , σ , k_i and a_i ($i = 1, 2$), are piecewisely positive constants. When v is piecewise constant, we denote its minimum and maximum values by $\underline{v} = \min_x v$ and $\bar{v} = \max_x v$, respectively. The coefficients κ_i , $i = 1, 2$ are defined as

$$\kappa_i = \sum_{m \in \{n, s, p\}} \kappa_{im}(c_1) \mathbf{1}_{\Omega_m}, \quad (2)$$

where $\kappa_{1m}, \kappa_{2m}: (0, +\infty) \rightarrow (0, +\infty)$. For the spherical particles in the electrode regions, we set the radii as $R_s = \sum_{m \in \{n, p\}} R_m \mathbf{1}_{\Omega_m}$ and the maximum lithium concentration as $c_{2, \max} = \sum_{m \in \{n, p\}} c_{2, \max, m} \mathbf{1}_{\Omega_m}$. The source term J depends on the lithium concentration at the particle surface, $\bar{c}_2(x, t) = c_2(x, R_s(x), t)$, and $\eta := \phi_2 - \phi_1 - U$, where $U = \sum_{m \in \{n, p\}} U_m(\bar{c}_2) \mathbf{1}_{\Omega_m}$, and $U_m: (0, c_{2, \max, m}) \rightarrow \mathbb{R}$. Then, J is expressed as

$$J = \sum_{m \in \{n, p\}} J_m(c_1, \bar{c}_2, \eta) \mathbf{1}_{\Omega_m}, \quad (3)$$

where $J_m: (0, +\infty) \times (0, c_{2, \max, m}) \times \mathbb{R} \rightarrow \mathbb{R}$. On the other hand, the function $f: (0, +\infty) \rightarrow \mathbb{R}$ is assumed to be independent of the spatial coordinates. The assumed domains of these functions imply the physical constraints $c_1 > 0$ and $0 < c_2 < c_{2, \max}$.

To complete the system, we introduce the initial conditions,

$$\begin{aligned} c_1(x, 0) &= c_{10}(x) > 0, \quad x \in \Omega_1, \\ c_2(x, r, 0) &= c_{20}(x, r), \quad 0 < c_{20}(x, r) < c_{2, \max}(x), \quad (x, r) \in \Omega_{2r}, \end{aligned}$$

the boundary conditions with a given function $I: \Gamma \rightarrow \mathbb{R}$ and a constant F ,

$$\begin{aligned}
& -(\kappa_1 \nabla \phi_1 - \kappa_2 \nabla f(c_1)) \cdot \mathbf{n}|_{\partial\Omega} = 0, \\
& -\sigma \nabla \phi_2 \cdot \mathbf{n}|_{\Gamma} = I, \quad -\sigma \nabla \phi_2 \cdot \mathbf{n}|_{\partial\Omega_2 \setminus \Gamma} = 0, \\
& -k_1 \nabla c_1 \cdot \mathbf{n}|_{\partial\Omega} = 0, \\
& -r^2 k_2 \frac{\partial c_2(x)}{\partial r} \Big|_{r=0} = 0, \quad -r^2 k_2 \frac{\partial c_2(x)}{\partial r} \Big|_{r=R_s(x)} = \frac{J(x)}{F}, \quad x \in \Omega_2, \quad (4)
\end{aligned}$$

and the interface conditions

$$\begin{aligned}
\llbracket \phi_1 \rrbracket|_{\Gamma_{sk}} &= 0, \quad \llbracket (\kappa_1 \nabla \phi_1 - \kappa_2 \nabla f(c_1)) \cdot \boldsymbol{\nu} \rrbracket|_{\Gamma_{sk}} = 0, \quad k \in \{\text{n}, \text{p}\}, \\
\llbracket c_1 \rrbracket|_{\Gamma_{sk}} &= 0, \quad \llbracket k_1 \nabla c_1 \cdot \boldsymbol{\nu} \rrbracket|_{\Gamma_{sk}} = 0, \quad k \in \{\text{n}, \text{p}\},
\end{aligned}$$

where \mathbf{n} denotes the outward unit normal vector, Γ is a measurable subset of $\partial\Omega_2$ with positive measure, Γ_{sn} and Γ_{sp} are the separator-negative and separator-positive interfaces respectively, $\llbracket v \rrbracket|_{\Sigma}$ represents the jump of a quantity v across the interface Σ , and $\boldsymbol{\nu}$ denotes the outward unit normal vector at $\partial\Omega_s$.

Note that the subsystem involving ϕ_1 and ϕ_2 forms a Neumann problem. For the existence of a solution, it is necessary that the following compatibility condition holds:

$$\int_{\Omega_2} a_2 J(t) \, dx = \int_{\Gamma} I(t) \, ds = 0. \quad (5)$$

Furthermore, to ensure the uniqueness of the solution, we impose the additional constraint:

$$\int_{\Omega} \phi_1 \, dx = 0. \quad (6)$$

Remark 1.1. Apart from making the coupling quasilinear by the coefficients (2), the coupling is influenced by the nonlinear function J on the right-hand side of (1) and the Neumann boundary condition (4), which represents the homogenization process and the electrochemical coupling between the electrode scale and the particle scale.

More specifically, the DFN model is a particular case of the more general mathematical formulation (1), when $\kappa_2 = \frac{2RT}{F} \kappa_1 (1 - t_+^0)$, $f = \ln$, and J is governed by the Butler-Volmer equation [13]. For a detailed derivation of the DFN model, we recommend referring to [2, 14, 15, 16, 17]. As noted by

[18], the change of variables for ϕ_1 is avoided in this paper, ensuring that the finite element error analysis in this original formulation is also applicable to non-uniform temperature distributions.

Assumption 1.1. $c_{10} \in L^2(\Omega)$, $c_{20} \in L^2(\Omega_2; L_r^2(0, R_s(\cdot)))$. $c_{10}(x) > 0$, $x \in \Omega_1$ a.e.; $0 < c_{20}(x, r) < c_{2,\max}(x)$, $(x, r) \in \Omega_{2r}$ a.e.. $I \in L^2(0, T; L^2(\Gamma))$ and satisfies the condition $\int_\Gamma I(t) ds = 0$, $t \in (0, T)$ a.e..

Assumption 1.2. $f \in C^1(0, +\infty)$. For $m \in \{n, p\}$, $\kappa_{1m}, \kappa_{2m} \in C^2(0, +\infty)$, $U_m \in C^2(0, c_{2,\max,m})$, $J_m \in C^1((0, +\infty) \times (0, c_{2,\max,m}) \times \mathbb{R})$ and

$$\exists \alpha > 0: \forall (c_1, \bar{c}_2, \eta) \in (0, +\infty) \times (0, c_{2,\max,m}) \times \mathbb{R}, \quad \frac{\partial J_m}{\partial \eta}(c_1, \bar{c}_2, \eta) \geq \alpha.$$

Given $T > 0$ and setting $\Omega_{1T} = \Omega_1 \times (0, T)$, $\Omega_{2rT} = \Omega_{2r} \times (0, T)$. With function spaces and notations introduced in Appendix A, the weak solution of (1) can be defined as a quadruplet $(\phi_1, \phi_2, c_1, c_2)$,

$$\begin{aligned} \phi_1 &\in L^2(0, T; H_*^1(\Omega)), \quad \phi_2 \in L^2(0, T; H^1(\Omega_2)), \\ c_1 &\in C([0, T]; L^2(\Omega)) \cap L^2(0, T; H^1(\Omega)), \quad \frac{\partial c_1}{\partial t} \in L^2(0, T; L^2(\Omega)), \\ c_2 &\in C([0, T]; L^2(\Omega_2; L_r^2(0, R_s(\cdot)))) \cap L^2(0, T; L^2(\Omega_2; H_r^1(0, R_s(\cdot)))) , \\ &\quad \frac{\partial c_2}{\partial t} \in L^2(0, T; L^2(\Omega_2; L_r^2(0, R_s(\cdot)))) , \end{aligned}$$

such that $c_1(0) = c_{10}$, $c_2(0) = c_{20}$, $\kappa_1, \kappa_2 \in L^\infty(\Omega_{1T})$, $f(c_1) \in L^2(0, T; H^1(\Omega))$, $J \in L^2(0, T; L^2(\Omega_2))$, $c_1(x, t) > 0$, $(x, t) \in \Omega_{1T}$ a.e., $0 < c_2(x, r, t) < c_{2,\max}(x)$, $(x, r, t) \in \Omega_{2rT}$ a.e., and for $t \in (0, T)$ a.e.,

$$\int_\Omega \kappa_1(t) \nabla \phi_1(t) \cdot \nabla \varphi dx - \int_\Omega \kappa_2(t) \nabla f(c_1(t)) \cdot \nabla \varphi dx - \int_{\Omega_2} a_2 J(t) \varphi dx = 0, \quad \forall \varphi \in H^1(\Omega), \quad (7)$$

$$\int_{\Omega_2} \sigma \nabla \phi_2(t) \cdot \nabla \varphi dx + \int_{\Omega_2} a_2 J(t) \varphi dx + \int_\Gamma I(t) \varphi ds = 0, \quad \forall \varphi \in H^1(\Omega_2), \quad (8)$$

$$\int_\Omega \varepsilon_1 \frac{dc_1}{dt}(t) \varphi dx + \int_\Omega k_1 \nabla c_1(t) \cdot \nabla \varphi dx - \int_{\Omega_2} a_1 J(t) \varphi dx = 0, \quad \forall \varphi \in H^1(\Omega), \quad (9)$$

$$\begin{aligned} & \int_{\Omega_2} \int_0^{R_s(x)} \frac{dc_2}{dt}(t) \psi r^2 dr dx + \int_{\Omega_2} \int_0^{R_s(x)} k_2 \frac{\partial c_2(t)}{\partial r} \frac{\partial \psi}{\partial r} r^2 dr dx + \\ & \int_{\Omega_2} \frac{R_s^2(x)}{F} J(x, t) \psi(x, R_s(x)) dx = 0, \quad \forall \psi \in L^2(\Omega_2; H_r^1(0, R_s(\cdot))). \end{aligned} \quad (10)$$

Remark 1.2. In certain contexts, it is more convenient to adopt an alternative formulation of (7)-(10), in particular by replacing (8) with the following variational equation:

$$\int_{\Omega_2} \sigma \nabla \phi_2(t) \cdot \nabla \varphi dx + \int_{\Omega_2} a_2 J(t) \varphi dx + \int_{\Gamma} I(t) \varphi ds = 0, \quad \forall \varphi \in H_*^1(\Omega_2), \quad (11)$$

where the test space coincides with the solution space. This formulation is particularly advantageous for establishing the existence of weak solutions (see [19, Proposition 2.16]). The equivalence between the two formulations follows from the compatibility condition (5). For consistency with the finite element semi-discrete error analysis developed in [18], we adopt the $H_*^1(\Omega)$ formulation (11) throughout the remainder of this paper.

Under a slightly more stringent version of Assumptions 1.1 and 1.2 with higher regularity, local existence and uniqueness of the solution to the DFN model for $\dim \Omega = 1$ was established by [20, 21]. Moreover, the solution can be extended to a globally unique solution under specific conditions [21]. However, the problem of existence and uniqueness remains open for the case of $\dim \Omega = 2, 3$. The main mathematical challenges in this context include the strongly nonlinear source terms with singular behaviour, discontinuous and nonlinear coefficients, the lack of smoothness of the boundary and the pseudo- $(N+1)$ -dimensional structure.

Efficient simulation of the DFN model continues to be an active area of research. Various spatial discretization methods have been employed to convert the system of PDEs to a system of DAEs. These include the finite element method [22, 13, 23, 16], finite difference method [2, 24, 25, 26], finite volume method [27, 28], collocation method [29, 30], and hybrid method [3, 31]. To achieve full discretization, computationally efficient time-stepping algorithms are applied, such as those detailed in [32, 13, 33, 34]. Among these methods, the finite element method is particularly advantageous for handling irregular geometries, unconventional boundary conditions, heterogeneous compositions, and ensuring global conservation. As a result, it is increasingly adopted in battery modeling software [33, 35, 36, 37]. Additionally,

the backward Euler method is commonly employed due to its unconditional stability [28, 38, 39, 35, 40, 41, 42].

Despite notable advancements in numerical methods for the DFN model, research on rigorous error analysis remains limited [23, 18]. The work in [23] was the first to present a convergence analysis of the backward Euler finite element discretization of this model. However, the analysis has limitations: it is inapplicable for the cases $N = 2, 3$, where the imbedding $H^1(D_2) \hookrightarrow C(\bar{D}_2)$ fails and it requires additional assumptions or efforts to validate the interpolation operator I_0^x used therein. Furthermore, the theoretical convergence rates presented do not align with observed numerical results. Recently, a novel approach to estimating the error for c_2 was proposed in [18]. This approach utilizes a multiscale or pseudo- $(N+1)$ -dimensional projection, which aligns the analysis with the established framework from [43]. Additionally, the inclusion of trace error estimation enabled proving optimal-order convergence concerning the radial mesh size. The primary aim of this paper is to extend the semi-discrete error analysis presented in [18] to the fully discrete setting, addressing the associated gaps in the backward Euler finite element scheme.

An efficient solver is also crucial for enhancing simulation efficiency in practical applications, particularly when full discretization leads to a large system of nonlinear algebraic equations. From a numerical algebra perspective, existing solvers can be categorized within the framework of the nonlinear Gauss-Seidel methods [44, 45], differing mainly in the way the problem is partitioned into blocks. Fully coupled solvers [24, 33, 39] solve all unknown variables simultaneously using Newton's method. This approach typically converges rapidly due to the comprehensive coupling of all equations, but it requires significant computational resources for solving the large-scale linear system at each Newton step. Decomposition solvers [9, 28, 46, 13, 42, 40] decompose the problem into small block subproblems, introducing an outer iteration loop to handle the coupling between them. Each subproblem may not be solved exactly, and an appropriate nonlinear solver may be used within an inner iteration loop. Generally, solvers with larger blocks, which couple more PDEs, tend to converge faster but increase storage and computational costs for solving subproblems. As emphasized in [47], understanding the problem's physics and the effect of coupling extent is crucial. To accommodate varying computational capabilities, it is essential to strike a balance between solution speed and computational efficiency, motivating the development of innovative decomposition strategies tailored to the system's characteristics.

The challenges in designing efficient solvers for the DFN model arise from the strong nonlinear reaction term and its multiscale nature. The reaction term J , governed by the Butler-Volmer equation [48], involves complex mathematical functions such as exponentials and power roots, which hinder convergence and reduce robustness in fully decomposition solvers [28, 42, 40]. To address these difficulties, both fully coupled and tailored decomposition [13] solvers have been developed, offering improved convergence and robustness. Furthermore, the multiscale pseudo- $(N+1)$ -dimensional equation introduces an additional dimension, significantly increasing computational scale and cost. This motivates efforts to decouple c_2 in the outer [9, 46, 13] or inner iterations [39]. Building on these challenges and insights, this paper also proposes a fast and robust solver that effectively controls memory usage.

The primary contributions of this paper are threefold. First, based on the finite element semi-discretization in [18], we propose the corresponding backward Euler finite element discretization and derive error estimates with optimal convergence rates for $N = 1, 2, 3$. Second, we introduce a novel solver that fully decouples the microscopic variable c_2 through two effective decoupling procedures, along with an optional decomposition strategy. These approaches significantly accelerate the solution process while keeping memory usage low, making the solver particularly suitable for large-scale 2D/3D problems. Finally, we validate the numerical convergence rates in 2D and 3D using real battery parameters and provide a comprehensive comparison with existing solvers. To the best of our knowledge, such numerical verification and comparison have not been previously reported in the literature.

The paper is structured as follows. Section 2 presents the backward Euler finite element discretization and derives error estimates with optimal convergence rates. Section 3 introduces the novel fast solver, detailing its key decoupling procedures and an optional decomposition strategy. Section 4 reports numerical experiments with real battery parameters to validate the error estimates and assess the solver's performance. Finally, conclusions are drawn in section 5.

2. Error analysis of the finite element fully-discrete problems

In this section, we only consider $\bar{\Omega}_m \subset \mathbb{R}^N$, $m \in \{\text{n, s, p}\}$ as polygonal domains such that $\bar{\Omega}_m$ is the union of a finite number of polyhedra. Let $\mathcal{T}_{h,m}$ be a regular family of triangulation for $\bar{\Omega}_m$, $m \in \{\text{n, s, p}\}$, and the meshes match at the interfaces, i.e., the points, edges and faces of discrete

elements fully coincide at the interface. Hence, $\mathcal{T}_h := \bigcup_{m \in \{n, s, p\}} \mathcal{T}_{h,m}$ and $\mathcal{T}_{2,h} := \bigcup_{m \in \{n, p\}} \mathcal{T}_{h,m}$ are also regular family of triangulations for $\bar{\Omega}$ and $\bar{\Omega}_2$ respectively. Additionally, it is assumed that all (K, P_K, Σ_K) , $K \in \mathcal{T}_h$, are finite element affine families [49]. For the closed interval $[0, R_s(x)]$, $x \in \Omega_2$, let $\mathcal{T}_{\Delta_r}(x)$ be a family of regular meshes, such that $[0, R_s(x)] = \bigcup_{I \in \mathcal{T}_{\Delta_r}(x)} I$. It is also assumed that each element of $\mathcal{T}_{\Delta_r}(x)$ is affine equivalent to a reference element. Since R_s is piecewise constant, here only two sets of meshes are considered, i.e.,

$$\mathcal{T}_{\Delta_r}(x) = \begin{cases} \mathcal{T}_{\Delta_r p}, & x \in \Omega_p, \\ \mathcal{T}_{\Delta_r n}, & x \in \Omega_n. \end{cases}$$

For each element $K \in \mathcal{T}_h$ and $I \in \bigcup_{x \in \Omega_2} \mathcal{T}_{\Delta_r}(x)$, we use h_K and Δr_I for the diameter respectively. Let $h = \max_{K \in \mathcal{T}_h} h_K$ and $\Delta r = \max_{I \in \bigcup_{x \in \Omega_2} \mathcal{T}_{\Delta_r}(x)} \Delta r_I$.

The unknowns ϕ_1 , ϕ_2 and c_1 are discretized by piecewise-linear elements. Let $V_h^{(1)}(\bar{\Omega})$ and $V_h^{(1)}(\bar{\Omega}_2)$ be the corresponding finite element spaces for c_1 and ϕ_2 , while

$$W_h(\bar{\Omega}) = \left\{ w_h \in V_h^{(1)}(\bar{\Omega}) : \int_{\Omega} w_h(x) dx = 0 \right\},$$

for ϕ_1 . For the pseudo- $(N+1)$ dimensional c_2 , piecewise-constant elements are used for discretization in the x coordinate while piecewise-linear elements in the r coordinate. Namely, a tensor product finite element space

$$V_{h\Delta r}(\bar{\Omega}_{2r}) := \left(V_h^{(0)}(\bar{\Omega}_n) \otimes V_{\Delta r}^{(1)}[0, R_n] \right) \bigcap \left(V_h^{(0)}(\bar{\Omega}_p) \otimes V_{\Delta r}^{(1)}[0, R_p] \right) \quad (12)$$

is used.

In order to obtain a full discretization, we consider a uniform mesh for the time variable t . Define $t_k := k\Delta t$, $k = 0, 1, \dots, K$, $\Delta t > 0$ being the time-step, and $K := [T/\Delta t]$, the integral part of $T/\Delta t$. By means of the backward Euler method, finite element fully discrete problems for (7)-(10) are proposed as follows:

Given $(c_{1h}^0, c_{2h\Delta r}^0) \in V_h^{(1)}(\bar{\Omega}) \times V_{h\Delta r}(\bar{\Omega}_{2r})$, $c_{1h}^0(x) > 0$, $0 < c_{2h\Delta r}^0(x, r) < c_{2,\max}(x)$, find $(\phi_{1h}^k, \phi_{2h}^k, c_{1h}^k, c_{2h\Delta r}^k) \in W_h(\bar{\Omega}) \times V_h^{(1)}(\bar{\Omega}_2) \times V_h^{(1)}(\bar{\Omega}) \times V_{h\Delta r}(\bar{\Omega}_{2r})$, $k = 1, \dots, K$, such that

$$\int_{\Omega} \kappa_{1h}^k \nabla \phi_{1h}^k \cdot \nabla w_h \, dx - \int_{\Omega} \kappa_{2h}^k \nabla f(c_{1h}^k) \cdot \nabla w_h \, dx - \int_{\Omega_2} a_2 J_h^k w_h \, dx = 0, \forall w_h \in W_h(\bar{\Omega}), \quad (13)$$

$$\int_{\Omega_2} \sigma \nabla \phi_{2h}^k \cdot \nabla v_h \, dx + \int_{\Omega_2} a_2 J_h^k v_h \, dx + \int_{\Gamma} I^k v_h \, dx = 0, \quad \forall v_h \in V_h^{(1)}(\bar{\Omega}_2), \quad (14)$$

$$\int_{\Omega} \varepsilon_1 \frac{c_{1h}^k - c_{1h}^{k-1}}{\tau} v_h \, dx + \int_{\Omega} k_1 \nabla c_{1h}^k \cdot \nabla v_h \, dx - \int_{\Omega_2} a_1 J_h^k v_h \, dx = 0, \quad \forall v_h \in V_h^{(1)}(\bar{\Omega}) \quad (15)$$

$$\begin{aligned} & \int_{\Omega_2} \int_0^{R_s(x)} \frac{c_{2h\Delta r}^k - c_{2h\Delta r}^{k-1}}{\tau} v_{h\Delta r} r^2 \, dr \, dx + \int_{\Omega_2} \int_0^{R_s(x)} k_2 \frac{\partial c_{2h\Delta r}^k}{\partial r} \frac{\partial v_{h\Delta r}}{\partial r} r^2 \, dr \, dx \\ & + \int_{\Omega_2} \frac{R_s^2(x)}{F} J_h^k(x) v_{h\Delta r}(x, R_s(x)) \, dx = 0, \quad \forall v_{h\Delta r} \in V_{h\Delta r}(\bar{\Omega}_{2r}), \end{aligned} \quad (16)$$

where

$$\kappa_{ih}^k = \sum_{m \in \{n, s, p\}} \kappa_{im}(c_{1h}^k) \mathbf{1}_{\Omega_m}, \quad i = 1, 2, \quad J_h^k = \sum_{m \in \{n, p\}} J_m(c_{1h}^k, \bar{c}_{2h}^k, \eta_h^k) \mathbf{1}_{\Omega_m},$$

$$\bar{c}_{2h}^k(x) := c_{2h\Delta r}^k(x, R_s(x)), \quad \eta_h^k = \phi_{2h}^k - \phi_{1h}^k - U_h^k, \quad U_h^k = \sum_{m \in \{n, p\}} U_m(\bar{c}_{2h}^k) \mathbf{1}_{\Omega_m}.$$

Remark 2.1. If the discrete compatibility condition

$$\int_{\Omega_2} a_2 J_h^k \, dx = \int_{\Gamma} I^k \, dx = 0 \quad (17)$$

holds, which is the discrete analogue of (5), then the finite element equation (13) is equivalent to

$$\int_{\Omega} \kappa_{1h}^k \nabla \phi_{1h}^k \cdot \nabla v_h \, dx - \int_{\Omega} \kappa_{2h}^k \nabla f(c_{1h}^k) \cdot \nabla v_h \, dx - \int_{\Omega_2} a_2 J_h^k v_h \, dx = 0, \quad \forall v_h \in V_h^{(1)}(\bar{\Omega}).$$

See Remark 4.1 for practical considerations regarding the preservation of this condition under numerical quadrature.

To present the finite element error analysis, we need to make the following assumptions.

Assumption 2.1.

$$c_{10} \in H_{\text{pw}}^2(\Omega_1), \quad c_{20} \in H^1(\Omega_2; H_r^1(0, R_s(\cdot))) \cap L^2(\Omega_2; H_r^2(0, R_s(\cdot))).$$

Assumption 2.2.

$$\phi_1 \in C([0, T]; H_{\text{pw}}^2(\Omega_1)), \phi_2 \in C([0, T]; H_{\text{pw}}^2(\Omega_2)), c_1 \in H^1(0, T; H_{\text{pw}}^2(\Omega_1)), \\ c_2 \in H^1(0, T; H^1(\Omega_2; H_r^1(0, R_s(\cdot))) \cap L^2(\Omega_2; H_r^2(0, R_s(\cdot)))).$$

Assumption 2.3. *There exist constants $L, M, N > 0$, such that for $t \in [0, T]$ a.e.,*

$$\|\phi_i(t)\|_{L^\infty(\Omega_i)}, \|\phi_{ih}(t)\|_{L^\infty(\Omega_i)}, \|\nabla \phi_i(t)\|_{L^\infty(\Omega_i)}, \|\nabla c_1(t)\|_{L^\infty(\Omega)} \leq L, i = 1, 2, \\ \frac{1}{M} \leq c_1(t), c_{1h}(t) \leq M, \quad \frac{1}{N} \leq \frac{\bar{c}_2(t)}{c_{2,\max}}, \frac{\bar{c}_{2h\Delta r}(t)}{c_{2,\max}} \leq \left(1 - \frac{1}{N}\right).$$

2.1. Auxiliary results

To analyze the finite element error for the multiscale system, it is essential to introduce several projection operators into finite element spaces, particularly tensor product spaces, along with their approximation properties.

Define the projection operator P_h from $H^1(\Omega)$ to $V_h^{(1)}(\bar{\Omega})$ such that $\forall u \in H^1(\Omega)$,

$$\int_{\Omega} k_1 \nabla(u - P_h u) \cdot \nabla \varphi_h \, dx + \int_{\Omega} (u - P_h u) \varphi_h \, dx = 0, \quad \forall \varphi_h \in V_h^{(1)}(\bar{\Omega}). \quad (18)$$

It is evident that P_h is well-defined, with the following approximation error [50]

$$\|u - P_h u\|_{H^1(\Omega)} \leq Ch \|u\|_{H_{\text{pw}}^2(\Omega_1)}. \quad (19)$$

Define the projection $P_{h\Delta r} : L^2(\Omega_2; H_r^1(0, R_s(\cdot))) \rightarrow V_{h\Delta r}(\bar{\Omega}_{2r})$,

$$\int_{\Omega_2} \int_0^{R_s(x)} \left(k_2 \frac{\partial(P_{h\Delta r} w - w)}{\partial r} \frac{\partial w_{h\Delta r}}{\partial r} + (P_{h\Delta r} w - w) w_{h\Delta r} \right) r^2 \, dr \, dx = 0, \\ \forall w_{h\Delta r} \in V_{h\Delta r}(\bar{\Omega}_{2r}), \quad (20)$$

and the projection error estimates [18] are given as follows:

Lemma 2.1. *If $w \in H^1(\Omega_2; H_r^1(0, R_s(\cdot))) \cap L^2(\Omega_2; H_r^2(0, R_s(\cdot)))$, then for $q = 0, 1$,*

$$\|w - P_{h\Delta r} w\|_{0, \Omega_2; q, r} \leq C(h \|w\|_{1, \Omega_2; 1, r} + (\Delta r)^{2-q} \|w\|_{0, \Omega_2; 2, r}).$$

Lemma 2.2. *If $w \in H^1(\Omega_2; H_r^1(0, R_s(\cdot))) \cap L^2(\Omega_2; H_r^2(0, R_s(\cdot)))$, we have*

$$\|(w - P_{h\Delta r}w)(\cdot, R_s(\cdot))\|_{0,\Omega_2} \leq C(h\|w\|_{1,\Omega_2;1,r} + (\Delta r)^2\|w\|_{0,\Omega_2;2,r}).$$

It can be seen from [18] that lemma 2.2 is crucial for establishing the optimal-order error estimates with respect to Δr .

2.2. Error estimation for c_1

By virtue of the projection operator P_h , the finite element error can be decomposed as follows:

$$c_1(t) - c_{1h}(t) = (c_1(t) - P_h c_1(t)) + (P_h c_1(t) - c_{1h}(t)) =: \rho_1(t) + \theta_1(t). \quad (21)$$

Since for $k = 0, 1$,

$$\|\rho_1(t)\|_{k,\Omega} \leq Ch\|c_1(t)\|_{2,\Omega_1} \leq Ch \left(\|c_{10}\|_{2,\Omega_1} + \int_0^t \left\| \frac{\partial c_1}{\partial t}(s) \right\|_{2,\Omega_1} ds \right), \quad (22)$$

it remains to estimate $\theta_1(t)$.

Next, since ε_1 is a piecewise positive constant function independent of time t , the norms $\left\| \varepsilon_1^{1/2} u \right\|_{L^2(\Omega)}$ and $\|u\|_{L^2(\Omega)}$ are equivalent. For simplicity, we assume $\varepsilon_1 \equiv 1$ in the subsequent analysis.

In addition, for a time-dependent variable $u(t)$, we use the notation $u^k = u(t_k)$ for brevity.

Lemma 2.3. *There exist an arbitrarily small number $\epsilon > 0$ and a positive constant C that do not depend on τ , h and Δr , such that for each $k = 1, \dots, K$,*

$$\begin{aligned} & \|\theta_1^k\|_{0,\Omega}^2 - \|\theta_1^{k-1}\|_{0,\Omega}^2 + \|\theta_1^k - \theta_1^{k-1}\|_{0,\Omega}^2 + 2\underline{k}_1\tau \|\nabla \theta^k\|_{0,\Omega}^2 \\ & \leq Ch^2 \left(\tau \|c_{10}\|_{2,\Omega_1}^2 + \tau \left\| \frac{\partial c_1}{\partial t} \right\|_{0;2,\Omega_1}^2 \right) + Ch^2 \left\| \frac{\partial c_1}{\partial t} \right\|_{0,k;2,\Omega_1}^2 + C\tau^2 \left\| \frac{\partial^2 c_1}{\partial t^2} \right\|_{0,k;0,\Omega}^2 \\ & \quad + C(\epsilon)\tau \|\theta_1^k\|_{0,\Omega}^2 + \epsilon\tau \left(\|\bar{c}_2^k - \bar{c}_{2h}^k\|_{0,\Omega_2}^2 + \|\phi_1^k - \phi_{1h}^k\|_{0,\Omega}^2 + \|\phi_2^k - \phi_{2h}^k\|_{0,\Omega_2}^2 \right). \end{aligned} \quad (23)$$

PROOF. The time derivative of c_1 at t_k is

$$\frac{\partial c_1}{\partial t}(t_k) = \frac{c_1(t_k) - c_1(t_{k-1})}{\tau} + \frac{1}{\tau} \int_{t_{k-1}}^{t_k} (s - t_{k-1}) \frac{\partial^2 c_1}{\partial t^2}(s) ds.$$

This leads to the decomposition of the temporal difference error as

$$\frac{\partial c_1}{\partial t}(t_k) - \frac{c_{1h}^k - c_{1h}^{k-1}}{\tau} = \frac{\rho_1^k - \rho_1^{k-1}}{\tau} + \frac{\theta_1^k - \theta_1^{k-1}}{\tau} + \int_{t_{k-1}}^{t_k} \left(\frac{s - t_{k-1}}{\tau} \right) \frac{\partial^2 c_1}{\partial t^2}(s) ds. \quad (24)$$

Hence taking $\varphi = v_h$ in (9) at $t = t_k$ and subtracting (15), it follows

$$\begin{aligned} & \int_{\Omega} (\theta_1^k - \theta_1^{k-1}) v_h dx + \tau \int_{\Omega} k_1 \nabla \theta_1^k \cdot \nabla v_h dx = \tau \int_{\Omega_2} a_1 (J^k - J_h^k) v_h dx dt \\ & - \int_{\Omega} (\rho_1^k - \rho_1^{k-1}) v_h dx - \int_{\Omega} \left(\int_{t_{k-1}}^{t_k} (s - t_{k-1}) \frac{\partial^2 c_1}{\partial t^2}(s) ds \right) v_h dx + \tau \int_{\Omega} \rho_1^k \cdot v_h dx. \end{aligned}$$

Next, by setting $v_h = \theta_1^k$, we have

$$\begin{aligned} & \frac{1}{2} \|\theta_1^k\|_{0,\Omega}^2 - \frac{1}{2} \|\theta_1^{k-1}\|_{0,\Omega}^2 + \frac{1}{2} \|\theta_1^k - \theta_1^{k-1}\|_{0,\Omega}^2 + k_1 \tau \|\nabla \theta_1^k\|_{0,\Omega}^2 \\ & \leq C \tau \|J^k - J_h^k\|_{0,\Omega_2} \|\theta_1^k\|_{0,\Omega} + C \|\rho_1^k - \rho_1^{k-1}\|_{0,\Omega} \|\theta_1^k\|_{0,\Omega} \\ & \quad + \tau^{\frac{3}{2}} \left\| \frac{\partial^2 c_1}{\partial t^2} \right\|_{0,k;0,\Omega} \|\theta_1^k\|_{0,\Omega} + \tau \|\rho_1^k\|_{0,\Omega} \|\theta_1^k\|_{0,\Omega}. \end{aligned} \quad (25)$$

Since Hypotheses 1.2 and 2.3 hold,

$$\begin{aligned} \|J^k - J_h^k\|_{0,\Omega_2} & \leq C \left(\|c_1^k - c_{1h}^k\|_{0,\Omega} + \|\bar{c}_2^k - \bar{c}_{2h}^k\|_{0,\Omega_2} + \|\phi_1^k - \phi_{1h}^k\|_{0,\Omega} + \|\phi_2^k - \phi_{2h}^k\|_{0,\Omega_2} \right) \\ & \leq C \left(\|\rho_1^k\|_{0,\Omega} + \|\theta_1^k\|_{0,\Omega} + \|\bar{c}_2^k - \bar{c}_{2h}^k\|_{0,\Omega_2} + \|\phi_1^k - \phi_{1h}^k\|_{0,\Omega} + \|\phi_2^k - \phi_{2h}^k\|_{0,\Omega_2} \right). \end{aligned} \quad (26)$$

We write

$$\rho_1^k - \rho_1^{k-1} = (I - P_h)(c_1^k - c_1^{k-1}) = (I - P_h) \int_{t_{k-1}}^{t_k} \frac{\partial c_1}{\partial t}(s) ds,$$

and obtain

$$\|\rho_1^k - \rho_1^{k-1}\|_{0,\Omega} \leq Ch \left\| \int_{t_{k-1}}^{t_k} \frac{\partial c_1}{\partial t}(s) ds \right\|_{2,\Omega_1} \leq Ch \tau^{\frac{1}{2}} \left\| \frac{\partial c_1}{\partial t} \right\|_{0,k;2,\Omega_1}.$$

By virtue of (22),

$$\|\rho_1^k\|_{0,\Omega} \leq Ch\|c_1(t_k)\|_{2,\Omega_1} \leq Ch\left(\|c_{10}\|_{2,\Omega_1} + \int_0^{t_k} \left\|\frac{\partial c_1}{\partial t}(s)\right\|_{2,\Omega_1} ds\right).$$

Together with the above estimates, Young's inequality implies that there exists $\epsilon > 0$, such that

$$\begin{aligned} & \|\theta_1^k\|_{0,\Omega}^2 - \|\theta_1^{k-1}\|_{0,\Omega}^2 + \|\theta_1^k - \theta_1^{k-1}\|_{0,\Omega}^2 + 2\underline{k}_1\tau \|\nabla\theta^k\|_{0,\Omega}^2 \\ & \leq Ch^2 \left(\tau\|c_{10}\|_{2,\Omega_1}^2 + \tau \left\|\frac{\partial c_1}{\partial t}\right\|_{0,2,\Omega_1}^2 \right) + Ch^2 \left\|\frac{\partial c_1}{\partial t}\right\|_{0,k;2,\Omega_1}^2 + C\tau^2 \left\|\frac{\partial^2 c_1}{\partial t^2}\right\|_{0,k;0,\Omega}^2 \\ & \quad + C(\epsilon)\tau \|\theta_1^k\|_{0,\Omega}^2 + \epsilon\tau \left(\|\bar{c}_2^k - \bar{c}_{2h}^k\|_{0,\Omega_2}^2 + \|\phi_1^k - \phi_{1h}^k\|_{0,\Omega}^2 + \|\phi_2^k - \phi_{2h}^k\|_{0,\Omega_2}^2 \right). \end{aligned}$$

2.3. Error estimation for c_2

Thanks to the projection operator $P_{h\Delta r}$, the finite element error for c_2 can be similarly decomposed as follows:

$$c_2(t) - c_{2h\Delta r}(t) = (c_2(t) - P_{h\Delta r}c_2(t)) + (P_{h\Delta r}c_2(t) - c_{2h\Delta r}(t)) =: \rho_2(t) + \theta_2(t), \quad (27)$$

and we have, setting $X = H^1(\Omega_2; H_r^1(0, R_s(\cdot))) \cap L^2(\Omega_2; H_r^2(0, R_s(\cdot)))$,

$$\begin{aligned} \|\rho_2(t)\|_{0,\Omega;q,r} & \leq Ch\|c_2(t)\|_{1,\Omega_2;1,r} + C(\Delta r)^{2-q}\|c_2(t)\|_{0,\Omega_2;q,r} \\ & \leq C(h + (\Delta r)^{2-q}) \left(\|c_{20}\|_X + \int_0^t \left\|\frac{\partial c_2}{\partial t}(s)\right\|_X ds \right), \quad q = 0, 1. \end{aligned} \quad (28)$$

We proceed to give an estimate for $\theta_2(t)$.

Lemma 2.4. *There exists an arbitrarily small number $\epsilon \in (0, 1)$ that does not depend on τ , h and Δr , such that for each $k = 1, \dots, K$,*

$$\begin{aligned} & \|\theta_2^k\|_{0,\Omega_2;0,r}^2 - \|\theta_2^{k-1}\|_{0,\Omega_2;0,r}^2 + \|\theta_2^k - \theta_2^{k-1}\|_{0,\Omega_2;0,r}^2 + 2\underline{k}_2\tau \left\|\frac{\partial\theta_2^k}{\partial r}\right\|_{0,\Omega_2;0,r}^2 \\ & \leq C(h^2 + (\Delta r)^4) \left(\tau\|c_{20}\|_X^2 + \tau \left\|\frac{\partial c_2}{\partial t}\right\|_{0,X}^2 + \left\|\frac{\partial c_2}{\partial t}\right\|_{0,k;X}^2 \right) + C\tau^2 \left\|\frac{\partial^2 c_2}{\partial t^2}\right\|_{0,k;0,\Omega_2;0,r}^2 \\ & \quad + C\epsilon\tau \left(\|c_1^k - c_{1h}^k\|_{0,\Omega}^2 + \|\phi_1^k - \phi_{1h}^k\|_{0,\Omega}^2 + \|\phi_2^k - \phi_{2h}^k\|_{0,\Omega_2}^2 \right) + C(\epsilon)\tau \|\theta_2^k\|_{0,\Omega_2;0,r}^2. \end{aligned} \quad (29)$$

PROOF. Similar to (24), the error of temporal difference can also be decomposed as

$$\frac{\partial c_2}{\partial t}(t_k) - \frac{c_{2h\Delta r}^k - c_{2h\Delta r}^{k-1}}{\tau} = \frac{\rho_2^k - \rho_2^{k-1}}{\tau} + \frac{\theta_2^k - \theta_2^{k-1}}{\tau} + \int_{t_{k-1}}^{t_k} \left(\frac{s - t_{k-1}}{\tau} \right) \frac{\partial^2 c_2}{\partial t^2}(s) \, ds.$$

Subtracting (16) from (10) at $t = t_k$, we obtain

$$\begin{aligned} & \int_{\Omega_2} \int_0^{R_s(x)} (\theta_2^k - \theta_2^{k-1}) v_{h\Delta r} r^2 \, dr \, dx + \tau \int_{\Omega_2} \int_0^{R_s(x)} k_2 \frac{\partial \theta_2^k}{\partial r} \frac{\partial v_{h\Delta r}}{\partial r} r^2 \, dr \, dx \\ &= - \int_{\Omega_2} \int_0^{R_s(x)} \left(\int_{t_{k-1}}^{t_k} (s - t_{k-1}) \frac{\partial^2 c_2}{\partial t^2}(s) \, ds \right) v_{h\Delta r} r^2 \, dr \, dx \, dt \\ & \quad - \int_{\Omega_2} \int_0^{R_s(x)} (\rho_2^k - \rho_2^{k-1}) v_{h\Delta r} r^2 \, dr \, dx + \tau \int_{\Omega_2} \int_0^{R_s(x)} \rho_2^k v_{h\Delta r} r^2 \, dr \, dx \\ & \quad - \tau \int_{\Omega_2} \frac{R_s^2}{F} (J^k - J_h^k) \bar{v}_h \, dx, \end{aligned} \tag{30}$$

where $\bar{v}_h := v_{h\Delta r}(x, R_s(x))$ and the penultimate term is due to (20).

We write

$$\rho_2^k - \rho_2^{k-1} = (I - P_{h\Delta r})(c_2^k - c_2^{k-1}) = (I - P_{h\Delta r}) \int_{t_{k-1}}^{t_k} \frac{\partial c_2}{\partial t}(s) \, ds,$$

and obtain

$$\|\rho_2^k - \rho_2^{k-1}\|_{0,\Omega_2;0,r} \leq C(h + (\Delta r)^2) \tau^{\frac{1}{2}} \left\| \frac{\partial c_2}{\partial t} \right\|_{0,k;X}.$$

For the last term, since $\|\bar{c}_2^k - \bar{c}_{2h}^k\|_{0,\Omega_2} \leq \|\bar{\rho}_2^k\|_{0,\Omega_2} + \|\bar{\theta}_2^k\|_{0,\Omega_2}$, it follows from (26) that

$$\begin{aligned} \|J^k - J_h^k\|_{0,\Omega_2} &\leq C \left(\|c_1^k - c_{1h}^k\|_{0,\Omega} + \|\bar{\rho}_2^k\|_{0,\Omega_2} + \|\bar{\theta}_2^k\|_{0,\Omega_2} \right. \\ &\quad \left. + \|\phi_1^k - \phi_{1h}^k\|_{0,\Omega} + \|\phi_2^k - \phi_{2h}^k\|_{0,\Omega_2} \right). \end{aligned} \tag{31}$$

By virtue of Lemma 2.2,

$$\begin{aligned} \|\bar{\rho}_2^k\|_{0,\Omega_2} &\leq Ch \|c_2(t_k)\|_{1,\Omega_2;1,r} + C(\Delta r)^2 \|c_2(t_k)\|_{0,\Omega_2;2,r} \\ &\leq C(h + (\Delta r)^2) \left(\|c_{20}\|_X + \int_0^{t_k} \left\| \frac{\partial c_2}{\partial t}(s) \right\|_X \, ds \right), \end{aligned} \tag{32}$$

and due to Proposition Appendix A.1, there is some $\epsilon_1 > 0$ to be determined later,

$$\|\bar{\theta}_2^k\|_{0,\Omega_2}^2 \leq \epsilon_1 \left\| \frac{\partial \theta_2^k}{\partial r} \right\|_{0,\Omega_2;0,r}^2 + C(\epsilon_1) \|\theta_2^k\|_{0,\Omega_2;0,r}^2. \quad (33)$$

Hence, Young's inequality yields for any $\epsilon_2 \in (0, 1)$,

$$\begin{aligned} \int_{t_{k-1}}^{t_k} \int_{\Omega_2} \frac{R_s^2}{F} (J^k - J_h^k) \bar{v}_h \, dx \, ds &\leq \epsilon_2 \tau \|J^k - J_h^k\|_{0,\Omega_2}^2 + C(\epsilon_2) \tau \|\bar{v}_h\|_{0,\Omega_2}^2 \\ &\leq C\tau (h^2 + (\Delta r)^4) \left(\|c_{20}\|_X^2 + \left\| \frac{\partial c_2}{\partial t} \right\|_{0,X}^2 \right) + C\epsilon_1 \tau \left\| \frac{\partial \theta_2^k}{\partial r} \right\|_{0,\Omega_2;0,r}^2 \\ &\quad + C\epsilon_2 \tau \left(\|c_1^k - c_{1h}^k\|_{0,\Omega}^2 + \|\phi_1^k - \phi_{1h}^k\|_{0,\Omega}^2 + \|\phi_2^k - \phi_{2h}^k\|_{0,\Omega_2}^2 \right) \\ &\quad + C(\epsilon_1) \tau \|\theta_2^k\|_{0,\Omega_2;0,r}^2 + C(\epsilon_2) \tau \|\bar{v}_h\|_{0,\Omega_2}^2. \end{aligned} \quad (34)$$

Finally, choosing $v_{h\Delta r} = \theta_2^k \in V_{h\Delta r}(\bar{\Omega}_{2r})$ in (30), and applying the Cauchy-Schwarz inequality along with (28), (33) and (34), we have

$$\begin{aligned} &\|\theta_2^k\|_{0,\Omega_2;0,r}^2 - \|\theta_2^{k-1}\|_{0,\Omega_2;0,r}^2 + \|\theta_2^k - \theta_2^{k-1}\|_{0,\Omega_2;0,r}^2 + 2\underline{k}_2 \tau \left\| \frac{\partial \theta_2^k}{\partial r} \right\|_{0,\Omega_2;0,r}^2 \\ &\leq C(h^2 + (\Delta r)^4) \left\| \frac{\partial c_2}{\partial t} \right\|_{0,k;X}^2 + C\tau (h^2 + (\Delta r)^4) \left(\|c_{20}\|_X^2 + \left\| \frac{\partial c_2}{\partial t} \right\|_{0,X}^2 \right) \\ &\quad + C\epsilon_2 \tau \left(\|c_1^k - c_{1h}^k\|_{0,\Omega}^2 + \|\phi_1^k - \phi_{1h}^k\|_{0,\Omega}^2 + \|\phi_2^k - \phi_{2h}^k\|_{0,\Omega_2}^2 \right) \\ &\quad + C(\epsilon_1, \epsilon_2) \tau \|\theta_2^k\|_{0,\Omega_2;0,r}^2 + C(\epsilon_2) \epsilon_1 \tau \left\| \frac{\partial \theta_2^k}{\partial r} \right\|_{0,\Omega_2;0,r}^2 + C\tau^2 \left\| \frac{\partial^2 c_2}{\partial t^2} \right\|_{0,k;0,\Omega_2;0,r}^2. \end{aligned}$$

Estimation (29) follows by choosing ϵ_1 sufficiently small.

2.4. Error estimation for the fully discrete problems

To this end, we still require error estimation for ϕ_1 and ϕ_2 , which will then be integrated with the previously derived results to address the fully coupled problem. The error estimations for ϕ_1 and ϕ_2 have already been provided in [18], and we restate the results here for completeness:

Proposition 2.1. *There is a constant C that does not depend on τ , h and Δr , such that*

$$\begin{aligned} & \|\phi_1(t_k) - \phi_{1h}^k\|_{1,\Omega}^2 + \|\phi_2(t_k) - \phi_{2h}^k\|_{1,\Omega_2}^2 \\ & \leq Ch^2 \left(\|\phi_1(t_k)\|_{2,\Omega_1}^2 + \|\phi_2(t_k)\|_{2,\Omega_2}^2 \right) \\ & \quad + C \left(\|c_1(t_k) - c_{1h}^k\|_{1,\Omega}^2 + \|\bar{c}_2(t_k) - \bar{c}_{2h}^k\|_{0,\Omega_2}^2 \right). \end{aligned}$$

Now, we are ready to establish the convergence result of this paper.

Theorem 2.1. *If Hypotheses 1.2-2.3 hold, there exists a constant C that does not depend on τ , h and Δr such that*

$$\begin{aligned} & \sum_{k=1}^K \tau \left(\|\phi_1^k - \phi_{1h}^k\|_{1,\Omega}^2 + \|\phi_2^k - \phi_{2h}^k\|_{1,\Omega_2}^2 + \|c_1^k - c_{1h}^k\|_{1,\Omega}^2 + \|\bar{c}_2^k - \bar{c}_{2h}^k\|_{0,\Omega_2}^2 \right) \\ & \leq C (h^2 + \tau^2 + (\Delta r)^4) + C \left(\|c_{10} - c_{10,h}\|_{0,\Omega}^2 + \|c_{20} - c_{20,h\Delta r}\|_{0,\Omega_2;0,r}^2 \right) \end{aligned} \quad (35)$$

$$\begin{aligned} & \sum_{k=1}^K \tau \|c_2^k - c_{2h\Delta r}^k\|_{0,\Omega_2;q,r}^2 \leq C (h^2 + \tau^2 + (\Delta r)^{4-2q}) \\ & \quad + C \left(\|c_{10} - c_{10,h}\|_{0,\Omega}^2 + \|c_{20} - c_{20,h\Delta r}\|_{0,\Omega_2;0,r}^2 \right), \quad q = 0, 1. \end{aligned} \quad (36)$$

PROOF. Combining Lemma 2.3 with Proposition 2.1, and utilizing (21), (22), (32) and (33), there is a constant ϵ_1 to be determined later, such that

$$\begin{aligned} & \|\theta_1^k\|_{0,\Omega}^2 - \|\theta_1^{k-1}\|_{0,\Omega}^2 + \|\theta_1^k - \theta_1^{k-1}\|_{0,\Omega}^2 + 2\underline{k}_1 \tau \|\nabla \theta^k\|_{0,\Omega}^2 \\ & \leq C(\epsilon_1) \tau \left(\|\theta_1^k\|_{0,\Omega}^2 + \|\theta_2^k\|_{0,\Omega_2;0,r}^2 \right) + C\epsilon_1 \tau \left(\|\nabla \theta_1^k\|_{0,\Omega}^2 + \left\| \frac{\partial \theta_2^k}{\partial r} \right\|_{0,\Omega_2;0,r}^2 \right) \\ & \quad + Ch^2 \left(\tau \|\phi_1^k\|_{2,\Omega_1}^2 + \tau \|\phi_2^k\|_{2,\Omega_2}^2 + \tau \|c_{10}\|_{2,\Omega_1}^2 + \tau \left\| \frac{\partial c_1}{\partial t} \right\|_{0;2,\Omega_1}^2 + \left\| \frac{\partial c_1}{\partial t} \right\|_{0,k;2,\Omega_1}^2 \right) \\ & \quad + C\tau^2 \left\| \frac{\partial^2 c_1}{\partial t^2} \right\|_{0,k;0,\Omega}^2 + C\tau (h^2 + (\Delta r)^4) \left(\|c_{20}\|_X^2 + \left\| \frac{\partial c_2}{\partial t} \right\|_{0;X}^2 \right). \end{aligned} \quad (37)$$

Again, combining Lemma 2.4 with Proposition 2.1, together with (21), (22), (32) and (33), there is also a constant $\epsilon_2 \in (0, 1)$ to be determined later, such that

$$\begin{aligned}
& \|\theta_2^k\|_{0,\Omega_2;0,r}^2 - \|\theta_2^{k-1}\|_{0,\Omega_2;0,r}^2 + \|\theta_2^k - \theta_2^{k-1}\|_{0,\Omega_2;0,r}^2 + 2\underline{k}_2\tau \left\| \frac{\partial\theta_2^k}{\partial r} \right\|_{0,\Omega_2;0,r}^2 \\
& \leq C(\epsilon_2)\tau \left(\|\theta_1^k\|_{0,\Omega}^2 + \|\theta_2^k\|_{0,\Omega_2;0,r}^2 \right) + C\epsilon_2\tau \left(\|\nabla\theta_1^k\|_{0,\Omega}^2 + \left\| \frac{\partial\theta_2^k}{\partial r} \right\|_{0,\Omega_2;0,r}^2 \right) \\
& \quad + C\tau h^2 \left(\|\phi_1^k\|_{2,\Omega_1}^2 + \|\phi_2^k\|_{2,\Omega_2}^2 + \|c_{10}\|_{2,\Omega_1}^2 + \left\| \frac{\partial c_1}{\partial t} \right\|_{0;2,\Omega_1}^2 \right) \\
& \quad + C(h^2 + (\Delta r)^4) \left(\tau \|c_{20}\|_X^2 + \tau \left\| \frac{\partial c_2}{\partial t} \right\|_{0;X}^2 + \left\| \frac{\partial c_2}{\partial t} \right\|_{0,k;X}^2 \right) \\
& \quad + C\tau^2 \left\| \frac{\partial^2 c_2}{\partial t^2} \right\|_{0,k;0,\Omega_2;0,r}^2.
\end{aligned} \tag{38}$$

Next, adding (37) and (38), and selecting ϵ_1, ϵ_2 sufficiently small, we have

$$\begin{aligned}
& \|\theta_1^k\|_{0,\Omega}^2 + \|\theta_2^k\|_{0,\Omega_2;0,r}^2 + \underline{k}_1\tau \|\nabla\theta_1^k\|_{0,\Omega}^2 + \underline{k}_2\tau \left\| \frac{\partial\theta_2^k}{\partial r} \right\|_{0,\Omega_2;0,r}^2 \\
& \leq \|\theta_1^{k-1}\|_{0,\Omega}^2 + \|\theta_2^{k-1}\|_{0,\Omega_2;0,r}^2 + C\tau \left(\|\theta_1^k\|_{0,\Omega}^2 + \|\theta_2^k\|_{0,\Omega_2;0,r}^2 \right) \\
& \quad + C\tau^2 \left(\left\| \frac{\partial^2 c_1}{\partial t^2} \right\|_{0,k;0,\Omega}^2 + \left\| \frac{\partial^2 c_2}{\partial t^2} \right\|_{0,k;0,\Omega_2;0,r}^2 \right) \\
& \quad + C\tau h^2 \left(\|\phi_1\|_{\infty;2,\Omega_1}^2 + \|\phi_2\|_{\infty;2,\Omega_2}^2 + \|c_{10}\|_{2,\Omega_1}^2 + \|c_{20}\|_X^2 \right) \\
& \quad + C\tau h^2 \left(\left\| \frac{\partial c_1}{\partial t} \right\|_{0;2,\Omega_1}^2 + \left\| \frac{\partial c_2}{\partial t} \right\|_{0;X}^2 \right) + C\tau(\Delta r)^4 \left(\|c_{20}\|_X^2 + \left\| \frac{\partial c_2}{\partial t} \right\|_{0;X}^2 \right) \\
& \quad + Ch^2 \left\| \frac{\partial c_1}{\partial t} \right\|_{0,k;2,\Omega_1}^2 + C(h^2 + (\Delta r)^4) \left\| \frac{\partial c_2}{\partial t} \right\|_{0,k;X}^2.
\end{aligned}$$

Discrete Gronwall's inequality yields

$$\begin{aligned}
& \|\theta_1^k\|_{0,\Omega}^2 + \|\theta_2^k\|_{0,\Omega_2;0,r}^2 + \sum_{l=1}^k \underline{k}_1 \tau \|\nabla \theta_1^l\|_{0,\Omega}^2 + \sum_{l=1}^k \underline{k}_2 \tau \left\| \frac{\partial \theta_2^l}{\partial r} \right\|_{0,\Omega_2;0,r}^2 \\
& \leq C \left(\|\theta_1^0\|_{0,\Omega}^2 + \|\theta_2^0\|_{0,\Omega_2;0,r}^2 \right) + C(\Delta r)^4 \left(\|c_{20}\|_X^2 + \left\| \frac{\partial c_2}{\partial t} \right\|_{0;X}^2 \right) \\
& \quad + Ch^2 \left(\|\phi_1\|_{\infty;2,\Omega_1}^2 + \|\phi_2\|_{\infty;2,\Omega_2}^2 + \|c_{10}\|_{2,\Omega_1}^2 + \|c_{20}\|_X^2 \right) \\
& \quad + Ch^2 \left(\left\| \frac{\partial c_1}{\partial t} \right\|_{0;2,\Omega_1}^2 + \left\| \frac{\partial c_2}{\partial t} \right\|_{0;X}^2 \right) + C\tau^2 \left(\left\| \frac{\partial^2 c_1}{\partial t^2} \right\|_{0;0,\Omega}^2 + \left\| \frac{\partial^2 c_2}{\partial t^2} \right\|_{0;0,\Omega_2;0,r}^2 \right) \\
& \leq C \left(\|\theta_1^0\|_{0,\Omega}^2 + \|\theta_2^0\|_{0,\Omega_2;0,r}^2 \right) + C(\tau^2 + h^2 + (\Delta r)^4).
\end{aligned}$$

Thus, we have the following $l^2(H^1)$ -norm estimation for c_1 , demonstrating the optimal order of convergence,

$$\begin{aligned}
\sum_{l=1}^k \tau \|c_1^l - c_{1h}^l\|_{1,\Omega}^2 & \leq \sum_{l=1}^k 2\tau \left(\|\rho_1^l\|_{1,\Omega}^2 + \|\theta_1^l\|_{0,\Omega}^2 + \|\nabla \theta_1^l\|_{0,\Omega}^2 \right) \\
& \leq Ch^2 + C\tau \sum_{l=1}^k \left(\|\theta_1^l\|_{0,\Omega}^2 + \|\nabla \theta_1^l\|_{0,\Omega}^2 \right) \\
& \leq C(\tau^2 + h^2 + (\Delta r)^4) + C \left(\|\theta_1^0\|_{0,\Omega}^2 + \|\theta_2^0\|_{0,\Omega_2;0,r}^2 \right),
\end{aligned}$$

and $l^2(L^2(H_r^q))$ -norm, $q = 0, 1$, for c_2

$$\begin{aligned}
\sum_{l=1}^k \tau \|c_2^l - c_{2h}^l\|_{0,\Omega_2;q,r}^2 & \leq \sum_{l=1}^k 2\tau \left(\|\rho_2^l\|_{0,\Omega_2;q,r}^2 + \|\theta_2^l\|_{0,\Omega_2;q,r}^2 \right) \\
& \leq C(\tau^2 + h^2 + (\Delta r)^{4-2q}) + C \left(\|\theta_1^0\|_{0,\Omega}^2 + \|\theta_2^0\|_{0,\Omega_2;0,r}^2 \right).
\end{aligned}$$

Further with $l^2(L^2)$ -norm estimation for \bar{c}_2 ,

$$\begin{aligned}
\sum_{l=1}^k \tau \|\bar{c}_2^l - \bar{c}_{2h}^l\|_{0,\Omega_2}^2 & \leq \sum_{l=1}^k C\tau \left(\|\bar{\rho}_2^l\|_{0,\Omega_2}^2 + \|\theta_2^l\|_{0,\Omega_2;0,r}^2 + \left\| \frac{\partial \theta_2^l}{\partial r} \right\|_{0,\Omega_2;0,r}^2 \right) \\
& \leq C(\tau^2 + h^2 + (\Delta r)^4) + C \left(\|\theta_1^0\|_{0,\Omega}^2 + \|\theta_2^0\|_{0,\Omega_2;0,r}^2 \right),
\end{aligned}$$

we also have $l^2(H^1)$ -norm estimation for ϕ_1 and ϕ_2 with the optimal order of convergence,

$$\begin{aligned}
& \sum_{t=1}^k \tau \|\phi_1^l - \phi_1^l\|_{1,\Omega}^2 + \tau \|\phi_2^l - \phi_2^l\|_{1,\Omega_2}^2 \\
& \leq Ch^2 \left(\|\phi_1\|_{\infty;2,\Omega_1}^2 + \|\phi_2\|_{\infty;2,\Omega_2}^2 \right) + C \sum_{l=1}^k \left(\tau \|c_1^l - c_{1h}^l\|_{1,\Omega}^2 + \tau \|\bar{c}_2^l - \bar{c}_{2h}^l\|_{0,\Omega_2}^2 \right) \\
& \leq C \left(\tau^2 + h^2 + (\Delta r)^4 \right) + C \left(\|\theta_1^0\|_{0,\Omega}^2 + \|\theta_2^0\|_{0,\Omega_2;0,r}^2 \right).
\end{aligned}$$

Finally, notice that triangle inequality yields

$$\begin{aligned}
\|\theta_1^0\|_{L^2(\Omega)} & \leq \|c_{10} - c_{1h}^0\|_{L^2(\Omega)} + Ch, \\
\|\theta_2^0\|_{L^2(\Omega_2;L_r^2(0,R_s(\cdot)))} & \leq \|c_{20} - c_{2h\Delta r}^0\|_{L^2(\Omega_2;L_r^2(0,R_s(\cdot)))} + C(h + (\Delta r)^2),
\end{aligned}$$

which completes the proof.

3. A twice decoupled solver

Let $(\phi_{1h}^{k-1}, \phi_{2h}^{k-1}, c_{1h}^{k-1}, c_{2h\Delta r}^{k-1})$ denote the fully discrete solution at the $(k-1)$ -th time step. In this section, we focus on efficiently solving the fully discrete system (13)–(16) to obtain the next solution tuple $(\phi_{1h}^k, \phi_{2h}^k, c_{1h}^k, c_{2h\Delta r}^k)$ at time step k .

We propose a novel, twice-decoupled fast solver to achieve this goal. The effectiveness and computational advantages of this approach will be demonstrated through numerical experiments in Subsection 4.2.

3.1. First decoupling: local inversion

Let $\{\chi_i \psi_j\}_{i=1,\dots,M_2}^{j=1,\dots,N_i}$ denote the basis functions for $V_{h\Delta r}(\bar{\Omega}_{2r})$, where $\chi_i = \mathbf{1}_{\hat{e}_i}$ and $\{\psi_j\}_{j=1,\dots,N_i}$ is the nodal basis for $V_{\Delta r}^{(1)}[0, R_m]$, for each $\hat{e}_i \in \mathcal{T}_{h,m}$, $m \in \{\text{n,p}\}$. Then the solution $c_{2h\Delta r}^k \in V_{h\Delta r}(\bar{\Omega}_{2r})$ can be expressed as

$$c_{2h\Delta r}^k(x, r) = \sum_{i=1}^{M_2} \sum_{j=1}^{N_i} c_{2h\Delta r,ij}^k \chi_i(x) \psi_j(r).$$

Substituting the test function $v_{h\Delta r}(x, r) = \chi_i(x)\psi_j(r)$ into (16), we obtain for each $\hat{e}_i \in \mathcal{T}_{2,h}$ the following equation:

$$\begin{aligned} & \int_0^{R_m} \frac{c_{2h\Delta r,il}^k - c_{2h\Delta r,il}^{k-1}}{\tau} \psi_l \psi_j r^2 dr + \int_0^{R_m} k_2 c_{2h\Delta r,il}^k \frac{\partial \psi_l}{\partial r} \frac{\partial \psi_j}{\partial r} r^2 dr \\ & + \frac{\delta_{jN_i}}{|\hat{e}_i|} \int_{\hat{e}_i} \left(\frac{R_m^2}{F} J_m(c_{1h}^k, c_{2h\Delta r,iN_i}^k, \phi_{2h}^k - \phi_{1h}^k - U_m(c_{2h\Delta r,iN_i}^k)) \right) dx = 0, \end{aligned} \quad (39)$$

where the Einstein summation convention is applied to index l . Equation (39) can be rewritten in matrix form as

$$AC_i^k - MC_i^{k-1} + J_{h,i}^k e_{N_i} = 0, \quad (40)$$

where $C_i^k = (c_{2h\Delta r,i1}^k, \dots, c_{2h\Delta r,iN_i}^k)^\top$, $C_i^{k-1} = (c_{2h\Delta r,i1}^{k-1}, \dots, c_{2h\Delta r,iN_i}^{k-1})^\top$, $e_{N_i} = [0, \dots, 0, 1]^\top \in \mathbb{R}^{N_i}$, $A = M + \tau K \in \mathbb{R}^{N_i \times N_i}$,

$$M_{ij} = \int_0^{R_m} \psi_i \psi_j r^2 dr, \quad K_{ij} = \int_0^{R_m} k_2 \frac{\partial \psi_i}{\partial r} \frac{\partial \psi_j}{\partial r} r^2 dr,$$

and the nonlinear function

$$J_{h,i}^k := \frac{\tau}{|\hat{e}_i|} \int_{\hat{e}_i} \left(\frac{R_m^2}{F} J_m(c_{1h}^k, c_{2h\Delta r,iN_i}^k, \phi_{2h}^k - \phi_{1h}^k - U_m(c_{2h\Delta r,iN_i}^k)) \right) dx.$$

Although only the N_i -th equation in (40) is nonlinear, it is coupled to the other linear equations via the matrix A . Since A is symmetric and positive definite, the system is equivalently written as

$$C_i^k - A^{-1}MC_i^{k-1} + J_{h,i}^k A^{-1}e_{N_i} = 0. \quad (41)$$

Taking the dot product with $e_{N_i}^\top$, we isolate the scalar nonlinear equation associated with the surface DOF $c_{2h\Delta r,iN_i}^k$:

$$c_{2h\Delta r,iN_i}^k + e_{N_i}^\top A^{-1}e_{N_i} J_{h,i}^k - e_{N_i}^\top A^{-1}MC_i^{k-1} = 0. \quad (42)$$

Due to the low order and tridiagonal structure of A , the matrix inversion is computationally inexpensive and can be efficiently carried out using algorithms like Thomas algorithm (TDMA) or cholesky decomposition.

This observation motivates a scale-decoupled solution strategy for the fully discrete system (13)–(16). First, we solve the decoupled system consisting of (13)–(15) and the scalar equations (42) to determine c_{1h}^k , ϕ_{1h}^k , ϕ_{2h}^k , and

the surface values $c_{2h\Delta r, iN_i}^k$ for $i = 1, \dots, M_2$. Then, using backward substitution into (40), we compute the remaining degrees of freedom in $c_{2h\Delta r}^k$. This approach is naturally parallelizable and significantly reduces the computational complexity by decoupling the spatial and particle-scale resolutions.

We now propose the following novel solver to efficiently handle the scale-coupled nonlinear system:

Step 1 (Decoupled global solve): Find $c_{1h}^k \in V_h^{(1)}(\bar{\Omega})$, $\phi_{1h}^k \in W_h(\bar{\Omega})$, $\phi_{2h}^k \in V_h^{(1)}(\bar{\Omega}_2)$, and $c_{2h\Delta r, iN_i}^k$, $i = 1, \dots, M_2$, such that for all $v_{1h} \in V_h^{(1)}(\bar{\Omega})$, $w_h \in W_h(\bar{\Omega})$, $v_{2h} \in V_h^{(1)}(\bar{\Omega}_2)$,

$$\int_{\Omega} \varepsilon_1 \frac{c_{1h}^k - c_{1h}^{k-1}}{\tau} v_{1h} dx + \int_{\Omega} k_1 \nabla c_{1h}^k \cdot \nabla v_{1h} dx - \int_{\Omega_2} a_1 J_h^k v_{1h} dx = 0, \quad (43)$$

$$\int_{\Omega} \kappa_{1h}^k \nabla \phi_{1h}^k \cdot \nabla w_h dx - \int_{\Omega} \kappa_{2h}^k \nabla f(c_{1h}^k) \cdot \nabla w_h dx - \int_{\Omega_2} a_2 J_h^k w_h dx = 0, \quad (44)$$

$$\int_{\Omega_2} \sigma \nabla \phi_{2h}^k \cdot \nabla v_{2h} dx + \int_{\Omega_2} a_2 J_h^k v_{2h} dx + \int_{\Gamma} I^k v_{2h} dx = 0, \quad (45)$$

$$c_{2h\Delta r, iN_i}^k + e_{N_i}^T A^{-1} e_{N_i} J_{h,i}^k - e_{N_i}^T A^{-1} M C_i^{k-1} = 0, \quad i = 1, \dots, M_2. \quad (46)$$

Step 2 (Local backward recovery): For each $i = 1, \dots, M_2$, recover the remaining degrees of freedom $c_{2h\Delta r, ij}^k$ for $j = N_i - 1, \dots, 1$, by solving the lower part of the linear system:

$$A C_i^k - M C_i^{k-1} + J_{h,i}^k e_{N_i} = 0. \quad (47)$$

Remark 3.1. Equation (46) constitutes M_2 independent nonlinear equations indexed by i . Owing to the tridiagonal structure of the matrix A in (47), once the surface value $c_{2h\Delta r, iN_i}^k$ is determined from **Step 1**, the remaining unknowns can be computed efficiently without invoking a direct or iterative linear solver. Specifically, one can use backward substitution from the $(N_i - 1)$ -th equation down to the first equation.

3.2. Second decoupling: Jacobian elimination

To solve the nonlinear system given by equations (43)-(46) (i.e., **Step 1** above), we employ Newton's method with a line search strategy:

1. (Initialization) Set the initial guess $X^0 := (c_{1h}^{k,0}, \phi_{1h}^{k,0}, \phi_{2h}^{k,0}, \bar{c}_{2h}^{k,0})$, typically as

$$\phi_{1h}^{k,0} = \phi_{1h}^{k-1}, \phi_{2h}^{k,0} = \phi_{2h}^{k-1}, c_{1h}^{k,0} = c_{1h}^{k-1}, \bar{c}_{2h}^{k,0} = c_{2h\Delta r}^{k-1}(\cdot, R_s(\cdot)).$$

Define the auxiliary quantities

$$U_h^{k,0} = \sum_{m \in \{n,p\}} U_m(\bar{c}_{2h}^{k,0}) \mathbf{1}_{\Omega_m}, \quad \eta_h^{k,0} = \phi_{2h}^{k,0} - \phi_{1h}^{k,0} - U_h^{k,0}.$$

Let $rtol$ denote the relative tolerance and set the iteration index $n = 1$.

2. (Newton Step) At each iteration n , compute the Newton direction d^n by solving the linear system

$$J^n d^n + F^n = 0, \quad (48)$$

where J^n and F^n are the Jacobian and residual evaluated at X^{n-1} .

3. (Line Search) Determine a step size γ^n using a line search algorithm, and update

$$X^n := X^{n-1} + \gamma^n d^n.$$

4. (Convergence Check) If $\left\| \frac{X^n - X^{n-1}}{X^{n-1}} \right\|_{l^\infty} < rtol$, terminate the iteration and set $\phi_{1h}^k = \phi_{1h}^{k,n}$, $\phi_{2h}^k = \phi_{2h}^{k,n}$, $c_{1h}^k = c_{1h}^{k,n}$, $\bar{c}_{2h}^k = \bar{c}_{2h}^{k,n}$. Otherwise, increment n and continue the iteration.

The main computational burden lies in solving the linear system (48). To define the residual vector F and Jacobian matrix J , we arrange the equations and degrees of freedom in the following order: c_{1h} , ϕ_{1h} , ϕ_{2h} and $c_{2h\Delta r, iN_i}^k$, $i = 1, \dots, M_2$. This ordering allows the residual vector to be expressed as

$$F = \begin{bmatrix} F_{c_1}^T & F_{\phi_1}^T & F_{\phi_2}^T & F_{c_{21}} & \cdots & F_{c_{2M_2}} \end{bmatrix}^T. \quad (49)$$

Here, the scalar function $F_{c_{2i}}$ represents the residual for the i -th equation in (46), while the i -th component of the vector function F_{c_1} , F_{ϕ_1} or F_{ϕ_2} corresponds to the residual obtained by choosing a nodal basis function φ_i associated with the respective degree of freedom as the test function in the variational formulation. For example,

$$(F_{c_1})_i = \int_{\Omega} \varepsilon_1 \frac{c_{1h}^k - c_{1h}^{k-1}}{\tau} \varphi_i dx + \int_{\Omega} k_1 \nabla c_{1h}^k \cdot \nabla \varphi_i dx - \int_{\Omega_2} a_1 J_h^k \varphi_i dx. \quad (50)$$

Grouping the variables into macroscopic $(c_{1h}, \phi_{1h}, \phi_{2h})$ and microscopic (\bar{c}_{2h})

components, the Jacobian matrix J can be expressed in the block form:

$$\left[\begin{array}{c|c} J_{\text{macro}} & U_{\text{src}} \\ \hline V_{\text{bdry}} & D_{\text{micro}} \end{array} \right] = \left[\begin{array}{ccc|cccc} J_{c_1 c_1} & J_{c_1 \phi_1} & J_{c_1 \phi_2} & u_{c_1 1} & u_{c_1 2} & \cdots & u_{c_1 M_2} \\ J_{\phi_1 c_1} & J_{\phi_1 \phi_1} & J_{\phi_1 \phi_2} & u_{\phi_1 1} & u_{\phi_1 2} & \cdots & u_{\phi_1 M_2} \\ J_{\phi_2 c_1} & J_{\phi_2 \phi_1} & J_{\phi_2 \phi_2} & u_{\phi_2 1} & u_{\phi_2 2} & \cdots & u_{\phi_2 M_2} \\ \hline v_{1 c_1} & v_{1 \phi_1} & v_{1 \phi_2} & w_{11} & 0 & \cdots & 0 \\ v_{2 c_1} & v_{2 \phi_1} & v_{2 \phi_2} & 0 & w_{22} & \cdots & 0 \\ \vdots & \vdots & \vdots & \vdots & \vdots & \ddots & \vdots \\ v_{M_2 c_1} & v_{M_2 \phi_1} & v_{M_2 \phi_2} & 0 & 0 & \cdots & w_{M_2 M_2} \end{array} \right]. \quad (51)$$

The subscript "src" indicates coupling due to source terms in equations (43)–(45), while "bdry" reflects contributions from particle-boundary conditions in (46). Each row of the latter block matrix in (51) corresponds to the Jacobian of a subvector of F . For example, the Jacobian of F_{c_1} is the first row block:

$$\left[J_{c_1 c_1} \quad J_{c_1 \phi_1} \quad J_{c_1 \phi_2} \quad u_{c_1 1} \quad u_{c_1 2} \quad \cdots \quad u_{c_1 M_2} \right],$$

where $J_{c_1 c_1}$, $J_{c_1 \phi_1}$, $J_{c_1 \phi_2}$ and $u_{c_1 j}$ denote the partial derivatives of F_{c_1} with respect to the degrees of freedom of c_{1h} , ϕ_{1h} , ϕ_{2h} and c_{2h,jN_j} , respectively. Similarly, the Jacobian of the i -th scalar residual $F_{c_2 i}$ is given by:

$$\left[v_{i c_1} \quad v_{i \phi_1} \quad v_{i \phi_2} \quad 0 \quad \cdots \quad w_{ii} \quad \cdots \quad 0 \right],$$

indicating coupling with all macroscopic variables and only the i -th microscopic surface unknown.

It is the spatial independence of $c_{2h\Delta r, iN_i}^{k,n}$ in (46) that leads to the diagonal D_{micro} . This fascinating structure allows a row transformation to reduce the Jacobian to lower-triangular form

$$\left[\begin{array}{cc} I & -U_{\text{src}} D_{\text{micro}}^{-1} \\ 0 & I \end{array} \right] \left[\begin{array}{cc} J_{\text{macro}} & U_{\text{src}} \\ V_{\text{bdry}} & D_{\text{micro}} \end{array} \right] = \left[\begin{array}{cc} J_{\text{macro}} - U_{\text{src}} D_{\text{micro}}^{-1} V_{\text{bdry}} & 0 \\ V_{\text{bdry}} & D_{\text{micro}} \end{array} \right].$$

Accordingly, the right-hand side is transformed as

$$F = \begin{bmatrix} F_1 \\ F_2 \end{bmatrix} \rightarrow \begin{bmatrix} F_1 - U_{\text{src}} D_{\text{micro}}^{-1} F_2 \\ F_2 \end{bmatrix}.$$

We can thus first solve a smaller linear system using the Schur complement of the block D_{micro} ,

$$J/D_{\text{micro}} = J_{\text{macro}} - U_{\text{src}} D_{\text{micro}}^{-1} V_{\text{bdry}}, \quad (52)$$

to obtain the Newton direction for c_{1h} , ϕ_{1h} and ϕ_{2h} , and then recover the direction for \bar{c}_{2h} through direct substitution.

Although D_{micro}^{-1} is trivial to compute due to its diagonal structure, it is still necessary to assess whether the associated elementary row transformations introduce significant fill-in or incur substantial computational cost. Fortunately, the following proposition demonstrates that the sparsity pattern of the Jacobian is preserved under this transformation.

Proposition 3.1. *The Schur complement J/D_{micro} shares the same sparsity pattern as J_{macro} .*

PROOF. Due to the diagonal structure of D_{micro} , if the entry

$$(U_{\text{src}} D_{\text{micro}}^{-1} V_{\text{bdry}})_{ij} = u_{ik} w_{kk} v_{kj} \neq 0$$

then there exists some $k \in \{1, 2, \dots, M_2\}$ such that both u_{ik} and v_{kj} are nonzero.

Let $\hat{e}_k \in \mathcal{T}_{2,h}$ and recall that P_1 elements are used to discretize c_1, ϕ_1 and ϕ_2 . Suppose the i -th degree of freedom of the full system corresponds to the $m(i)$ -th degree of freedom of variable $\xi(i) \in \{c_1, \phi_1, \phi_2\}$, denoted by $\xi(i)_{m(i)}$, associated with the global nodal basis $\varphi_{l(i)}$. Then

$$u_{ik} = (u_{\xi(i)k})_{m(i)} = \frac{\partial R_{\xi(i)k}}{\partial c_{2h\Delta r, kN_k}},$$

where $R_{\xi(i)k} = \int_{\hat{e}_k} a J_m(c_{1h}, c_{2h\Delta r, kN_k}, \phi_{2h} - \phi_{1h} - U_m(c_{2h\Delta r, kN_k})) \varphi_{l(i)} dx$, with $a \in \{-a_1, -a_2, a_2\}$. Similarly,

$$v_{ki} = (v_{k\xi(i)})_{m(i)} = \frac{\partial J_k}{\partial \xi(i)_{m(i)}},$$

where $J_k = \frac{\tau R_m^2(A^{-1})_{N_k N_k}}{|\hat{e}_k|F} \int_{\hat{e}_k} J_m(c_{1h}, c_{2h\Delta r, kN_k}, \phi_{2h} - \phi_{1h} - U_m(c_{2h\Delta r, kN_k})) dx$.

Hence, a nonzero entry $(U_{\text{src}} D_{\text{micro}}^{-1} V_{\text{bdry}})_{ij}$ may only arise if both the i -th and j -th degrees of freedom of the full system are associated with basis functions supported on the same element $\hat{e}_k \in \mathcal{T}_{2,h}$. In such cases, the entry (i, j) of J_{macro} , namely $(J_{\xi(i)\xi(j)})_{m(i)m(j)}$, already exists due to the contribution of the nonlinear term $R_{\xi(i)k}$ through the derivative $\frac{\partial R_{\xi(i)k}}{\partial \xi(j)_{m(j)}}$.

Proposition 3.1 implies that nonzero entries of $U_{\text{src}} D_{\text{micro}}^{-1} V_{\text{bdry}}$ are element-wise localized and thus sparse. From an implementation perspective, the full Jacobian J does not need to be constructed explicitly. The elimination can be performed element by element (see Algorithm 1) to directly form J/D_{micro} . Therefore, the computational cost of this elimination process is relatively small. We may thus safely conclude that the proposed decoupling strategy significantly reduces memory consumption and accelerates the solution procedure.

Algorithm 1 Jacobian elimination

```

1: Input: Original sub-Jacobian  $J_{\text{macro}}$ 
2: for each element  $\hat{e}_i$  in  $\mathcal{T}_{2,h}$  do
3:   Compute  $v_{ic_1}$ ,  $v_{i\phi_1}$ ,  $v_{i\phi_2}$  and  $w_{ii}$ 
4:   for each variable  $\xi$  in  $\{c_1, \phi_1, \phi_2\}$  do
5:     Get the index set of local degrees of freedom  $\{i_1, \dots, i_P\}$ 
6:     for each index  $j$  in  $\{i_1, \dots, i_P\}$  do
7:       Compute  $(u_{\xi i})_j$ 
8:        $(J_{\xi c_1}, J_{\xi \phi_1}, J_{\xi \phi_2})_j = (J_{\xi c_1}, J_{\xi \phi_1}, J_{\xi \phi_2})_j - \frac{1}{w_{ii}}(u_{\xi i})_j(v_{ic_1}, v_{i\phi_1}, v_{i\phi_2})$ 
9:     end for
10:  end for
11: end for

```

3.3. An optional nonlinear Gauss-Seidel decomposition

In the DFN model, the source term (3) is governed by the Butler-Volmer equation, which takes the following form:

$$J_m = k_m c_1^{\alpha_{a,m}} (c_{2,\max} - \bar{c}_2)^{\alpha_{a,m}} \bar{c}_2^{\alpha_{c,m}} \left(\exp\left(\frac{\alpha_{a,m} F}{RT_0} \eta_m\right) - \exp\left(\frac{-\alpha_{c,m} F}{RT_0} \eta_m\right) \right),$$

where $\alpha_{a,m} \in (0, 1)$, $\alpha_{c,m} \in (0, 1)$, k_m , F , R , T_0 are positive constants. The overpotential η_m is defined as

$$\eta_m = \phi_2 - \phi_1 - U_m(\bar{c}_2).$$

As seen in equations of (1), the system is coupled through J . Since the overpotential η appears inside exponential functions, even small variations in ϕ_1 , ϕ_2 or \bar{c}_2 can lead to large changes in J . This sensitivity can cause considerable fluctuations during each iteration and may lead to an excessive number

of outer iteration steps, when an inappropriate nonlinear Gauss-Seidel decomposition is used to solve (43)–(46). In fact, numerical experiments have confirmed this observation, supporting our conjecture.

This behavior motivates us to introduce an optional nonlinear Gauss-Seidel decomposition in **Step 1**, designed to balance speed and memory usage. In this strategy, the variables ϕ_1 , ϕ_2 and \bar{c}_2 are solved simultaneously, followed by an outer iteration to couple them with the remaining variable c_1 .

Step 1-Eta-0 (Initialization): Set the initial value of iteration, $X^0 := (c_{1h}^{k,0}, \phi_{1h}^{k,0}, \phi_{2h}^{k,0}, \bar{c}_{2h}^{k,0})$, typically as

$$\phi_{1h}^{k,0} = \phi_{1h}^{k-1}, \phi_{2h}^{k,0} = \phi_{2h}^{k-1}, c_{1h}^{k,0} = c_{1h}^{k-1}, \bar{c}_{2h}^{k,0} = c_{2h\Delta r}^{k-1}(\cdot, R_s(\cdot)).$$

Define the auxiliary quantities

$$U_h^{k,0} = \sum_{m \in \{n,p\}} U_m(\bar{c}_{2h}^{k,0}) \mathbf{1}_{\Omega_m}, \quad \eta_h^{k,0} = \phi_{2h}^{k,0} - \phi_{1h}^{k,0} - U_h^{k,0}.$$

Let $rtol$ be the relative tolerance and set the iteration index $n = 1$.

Step 1-Eta-1 (Subproblem (c_1)): Find $c_{1h}^{k,n} \in V_h^{(1)}(\bar{\Omega})$, such that for all $v_h \in V_h^{(1)}(\bar{\Omega})$,

$$\begin{aligned} \int_{\Omega} \varepsilon_1 \frac{c_{1h}^{k,n} - c_{1h}^{k-1}}{\tau} v_h \, dx + \int_{\Omega} k_1 \nabla c_{1h}^{k,n} \cdot \nabla v_h \, dx \\ - \int_{\Omega_2} \left(\sum_{m \in \{n,p\}} a_1 J_m(c_{1h}^{k,n}, \bar{c}_{2h}^{k,n-1}, \eta_h^{k,n-1}) \mathbf{1}_{\Omega_m} \right) v_h \, dx = 0. \end{aligned} \quad (53)$$

Step 1-Eta-2 (Subproblem $(\phi_1, \phi_2, \bar{c}_2)$): Find $\phi_{1h}^{k,n} \in W_h(\bar{\Omega})$, $\phi_{2h}^{k,n} \in V_h^{(1)}(\bar{\Omega}_2)$ and $c_{2h\Delta r, iN_i}^{k,n}$, $i = 1, \dots, M_2$, such that for all $w_h \in W_h(\bar{\Omega})$, $v_h \in V_h^{(1)}(\bar{\Omega}_2)$,

$$\int_{\Omega} \kappa_{1h}^{k,n} \nabla \phi_{1h}^{k,n} \cdot \nabla w_h \, dx - \int_{\Omega} \kappa_{2h}^{k,n} \nabla f(c_{1h}^{k,n}) \cdot \nabla w_h \, dx - \int_{\Omega_2} a_2 J_h^{k,n} w_h \, dx = 0, \quad (54)$$

$$\int_{\Omega_2} \sigma \nabla \phi_{2h}^{k,n} \cdot \nabla v_h \, dx + \int_{\Omega_2} a_2 J_h^{k,n} v_h \, dx + \int_{\Gamma} I^k v_h \, dx = 0, \quad (55)$$

$$c_{2h\Delta r, iN_i}^{k,n} + e_{N_i}^T A^{-1} e_{N_i} J_{h,i}^{k,n} - e_{N_i}^T A^{-1} M C_i^{k-1} = 0, \quad i = 1, \dots, M_2. \quad (56)$$

Step 1-Eta-3 (Convergence Check): Set $X^n := (c_{1h}^{k,n}, \phi_{1h}^{k,n}, \phi_{2h}^{k,n}, \bar{c}_{2h}^{k,n})$. If $\left\| \frac{X^n - X^{n-1}}{X^{n-1}} \right\|_{l^\infty} < rtol$, then terminate the iteration and set $\phi_{1h}^k = \phi_{1h}^{k,n}$, $\phi_{2h}^k = \phi_{2h}^{k,n}$, $c_{1h}^k = c_{1h}^{k,n}$, $\bar{c}_{2h}^k = \bar{c}_{2h}^{k,n}$. Otherwise, set $n = n + 1$ and return to **Step 1-Eta-1**.

4. Numerical experiments

To validate the theoretical analysis and demonstrate the superiority of the proposed solver, we present numerical simulations of the DFN model using real battery parameters from [3, 16]. These simulations were implemented using an in-house finite element code based on the libMesh library [51]. The computations were carried out on the high-performance computers of the State Key Laboratory of Scientific and Engineering Computing, Chinese Academy of Sciences.

Remark 4.1. To preserve the conservation property (5) in the fully discrete setting, we must ensure the following condition holds:

$$\int_{\Omega_2} a_2 J_h^k dx = \int_{\Gamma} I^k dx = 0.$$

In our galvanostatic simulations, I^k is a prescribed constant, so the condition $\int_{\Gamma} I^k dx = 0$ is satisfied exactly, even when numerical quadrature is used to compute the integral $\int_{\Gamma} I^k v_h dx$ in (14). For more general cases, we propose the following projection to enforce exact conservation:

$$I_*^k = I^k - \frac{1}{|\Gamma|} \int_{\Gamma} I^k dx.$$

Alternatively, one may employ a sufficiently accurate quadrature rule to approximate the integral reliably. Since the scheme is fully implicit, the condition $\int_{\Omega_2} a_2 J_h^k dx = 0$ is enforced indirectly via tight residual control in the nonlinear solver, thus maintaining conservation up to a high numerical tolerance in the sense of the chosen quadrature rule.

Remark 4.2. To compute $(\phi_{1h}^k, \phi_{2h}^k) \in W_h(\bar{\Omega}) \times V_h^1(\bar{\Omega}_2)$, we adopt the fixing one-point method, which is a practical variant of the null-space method. Specifically, we first solve the system in $V_h^1(\bar{\Omega}) \times V_h^1(\bar{\Omega}_2)$ by prescribing the

value of ϕ_{2h}^k to be zero at a chosen node. Then, we shift the resulting solution into the desired space $W_h(\bar{\Omega}) \times V_h^1(\bar{\Omega}_2)$ by subtracting the mean of ϕ_{1h}^k over the domain:

$$C = -\frac{1}{|\Omega|} \int_{\Omega} \phi_{1h}^k dx.$$

This procedure avoid constructing a basis for $W_h(\bar{\Omega})$. In fact, the matrix system is assembled using the standard nodal basis of $V_h^1(\bar{\Omega})$, and is obtained by simply deleting the row and column associated with the fixed point from the original singular matrix, as detailed in [52, Sec. 5.2.1].

4.1. Convergence validation

Due to computational resource limitations, complete validation of the convergence order for the P3D model is reported here while partial results for the P4D model can be found in Appendix B.

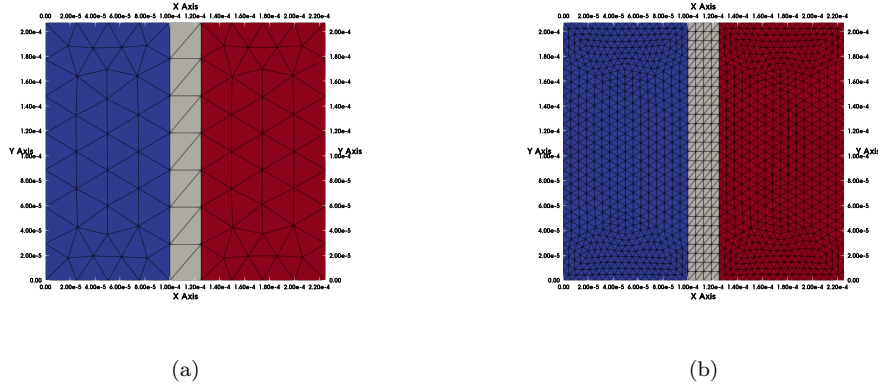


Figure 2: Spatial meshes for convergence verification. (a) Initial coarse mesh ($R_h = 0$). (b) Uniformly refined mesh ($R_h = 2$).

In this example, we set $\Omega_n = [0, 100] \times [0, 207]$, $\Omega_s = [100, 125] \times [0, 207]$, and $\Omega_p = [125, 225] \times [0, 207]$ (all dimensions in 10^{-6}m). The boundary Γ is defined as $\Gamma_n \cup \Gamma_p$, where $\Gamma_n = \{0\} \times [0, 207]$ and $\Gamma_p = \{225\} \times [0, 207]$. A 1C discharge rate is applied, using parameters from [16].

The initial spatial mesh, shown in Figure 2a, is refined uniformly with level R_h . The radial grid is initially uniform, with grid size $\Delta r = 1.25 \times 10^{-6}\text{m}$ and refinement level $R_{\Delta r}$. Since the exact solution is unknown, we use the finite element solution on a very fine mesh ($R_h = 5$, $R_{\Delta r} = 5$) with a sufficiently small step size $\tau_{\text{ref}} = 0.0390625\text{s}$ as a reference.

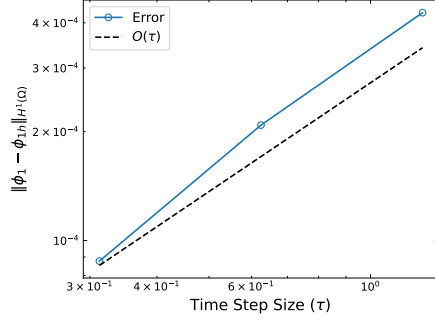
Figure 3 illustrates the absolute errors as a function of the time step size τ for all variables, evaluated at $T = 1.25s$ with $R_h = 5$ and $R_{\Delta r} = 5$ fixed. For fixed $R_{\Delta r} = 5$ ($R_h = 5$) and $\tau = \tau_{\text{ref}}$, we refine the initial mesh from $R_h = 1$ ($R_{\Delta r} = 1$) to $R_h = 3$ ($R_{\Delta r} = 3$). The error and convergence order with respect to h (Δr) at time $t_k = k\Delta t$ are summarized in Table 1 (Table 2). The observed convergence rates agree with our theoretical analysis.

Table 1: Error and convergence order for h .

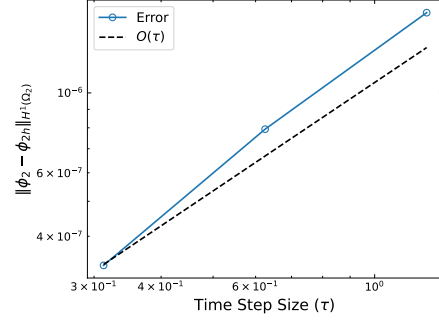
(a) $\ \phi_1(\cdot, t_k) - \phi_{1h}^k\ _{H^1(\Omega)}$					(b) $\ \phi_2(\cdot, t_k) - \phi_{2h}^k\ _{H^1(\Omega_2)}$				
k	$R_h = 1$	$R_h = 2$	$R_h = 3$	Order	k	$R_h = 1$	$R_h = 2$	$R_h = 3$	Order
2	9.90E-04	4.92E-04	2.40E-04	1.04	2	3.32E-05	1.65E-05	8.06E-06	1.03
4	9.90E-04	4.90E-04	2.39E-04	1.04	4	3.32E-05	1.65E-05	8.06E-06	1.03
6	1.02E-03	5.06E-04	2.47E-04	1.04	6	3.32E-05	1.65E-05	8.06E-06	1.03
8	1.06E-03	5.25E-04	2.56E-04	1.04	8	3.32E-05	1.65E-05	8.06E-06	1.03
10	1.05E-03	5.19E-04	2.53E-04	1.04	10	3.32E-05	1.65E-05	8.06E-06	1.03
(c) $\ c_1(\cdot, t_k) - c_{1h}^k\ _{H^1(\Omega)}$					(d) $\ \bar{c}_2(\cdot, t_k) - \bar{c}_{2h}^k\ _{L^2(\Omega_2)}$				
k	$R_h = 1$	$R_h = 2$	$R_h = 3$	Order	k	$R_h = 1$	$R_h = 2$	$R_h = 3$	Order
2	4.24E+00	2.25E+00	1.11E+00	1.02	2	1.36E-02	6.77E-03	3.31E-03	1.04
4	4.70E+00	2.37E+00	1.16E+00	1.03	4	2.96E-03	1.47E-03	7.18E-04	1.04
6	5.70E+00	2.89E+00	1.42E+00	1.03	6	7.91E-03	3.94E-03	1.92E-03	1.03
8	6.80E+00	3.42E+00	1.68E+00	1.03	8	1.73E-02	8.63E-03	4.21E-03	1.04
10	6.83E+00	3.40E+00	1.66E+00	1.04	10	1.21E-02	5.99E-03	2.92E-03	1.03
(e) $\ c_2(\cdot, t_k) - c_{2h\Delta r}^k\ _{L^2(\Omega_2; H_r^1(0, R_s(\cdot)))}$					(f) $\ c_2(\cdot, t_k) - c_{2h\Delta r}^k\ _{L^2(\Omega_2; L_r^2(0, R_s(\cdot)))}$				
k	$R_h = 1$	$R_h = 2$	$R_h = 3$	Order	k	$R_h = 1$	$R_h = 2$	$R_h = 3$	Order
2	2.45E-05	1.22E-05	5.94E-06	1.03	2	3.44E-12	1.71E-12	8.35E-13	1.04
4	9.85E-06	4.89E-06	2.39E-06	1.04	4	2.01E-12	9.97E-13	4.87E-13	1.04
6	1.16E-05	5.81E-06	2.84E-06	1.03	6	2.43E-12	1.21E-12	5.91E-13	1.03
8	2.71E-05	1.36E-05	6.62E-06	1.04	8	4.85E-12	2.42E-12	1.18E-12	1.04
10	1.86E-05	9.26E-06	4.52E-06	1.03	10	4.59E-12	2.28E-12	1.11E-12	1.03

4.2. Performance comparison

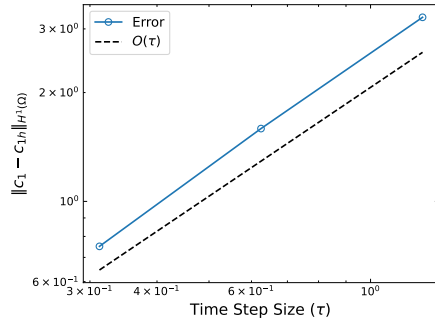
In this section, we compare the performance of several solvers, including the newly proposed fully coupled solver (referred to as "2DS-FC"), the



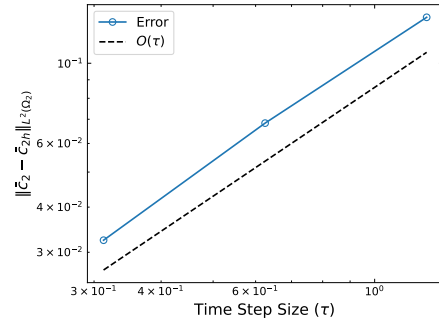
(a)



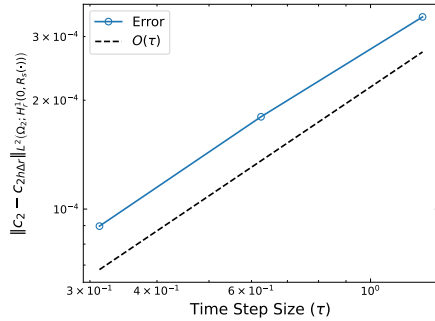
(b)



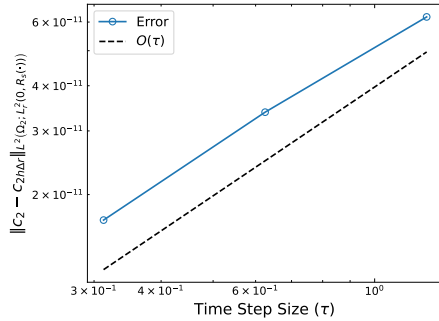
(c)



(d)



(e)



(f)

Figure 3: Time convergence obtained at $t = 1.25$ s. (a) Error for ϕ_1 in the H^1 -norm. (b) Error for ϕ_2 in the H^1 -norm. (c) Error for c_1 in the H^1 -norm. (d) Error for \bar{c}_2 in the L^2 -norm. (e) Error for c_2 in the $L^2(H_r^1)$ -norm. (f) Error for c_2 in the $L^2(L_r^2)$ -norm.

Table 2: Error and convergence order for r .

(a) $\ \phi_1(\cdot, t_k) - \phi_{1h}^k\ _{H^1(\Omega)}$					(b) $\ \phi_2(\cdot, t_k) - \phi_{2h}^k\ _{H^1(\Omega_2)}$				
k	$R_h = 1$	$R_h = 2$	$R_h = 3$	Order	k	$R_h = 1$	$R_h = 2$	$R_h = 3$	Order
2	1.33E-05	3.04E-06	7.09E-07	2.10	2	5.52E-08	1.28E-08	2.99E-09	2.10
4	1.86E-05	4.58E-06	1.08E-06	2.08	4	7.75E-08	1.89E-08	4.46E-09	2.08
6	5.07E-06	1.32E-06	3.15E-07	2.06	6	2.10E-08	5.40E-09	1.29E-09	2.07
8	2.60E-06	6.31E-07	1.50E-07	2.07	8	1.01E-08	2.44E-09	5.80E-10	2.07
10	4.99E-06	1.31E-06	3.14E-07	2.06	10	1.89E-08	4.98E-09	1.19E-09	2.06
(c) $\ c_1(\cdot, t_k) - c_{1h}^k\ _{H^1(\Omega)}$					(d) $\ \bar{c}_2(\cdot, t_k) - \bar{c}_{2h}^k\ _{L^2(\Omega_2)}$				
k	$R_h = 1$	$R_h = 2$	$R_h = 3$	Order	k	$R_h = 1$	$R_h = 2$	$R_h = 3$	Order
2	1.87E-02	4.34E-03	1.02E-03	2.10	2	4.20E-03	1.01E-03	2.38E-04	2.08
4	9.75E-03	2.49E-03	5.93E-04	2.07	4	1.94E-03	4.41E-04	1.05E-04	2.08
6	2.15E-03	5.88E-04	1.42E-04	2.05	6	1.38E-03	3.25E-04	7.74E-05	2.07
8	8.44E-03	2.03E-03	4.84E-04	2.07	8	1.08E-03	2.54E-04	6.05E-05	2.07
10	1.09E-02	2.75E-03	6.57E-04	2.07	10	9.64E-04	2.28E-04	5.44E-05	2.07
(e) $\ c_2(\cdot, t_k) - c_{2h\Delta r}^k\ _{L^2(\Omega_2; H_r^1(0, R_\#(\cdot)))}$					(f) $\ c_2(\cdot, t_k) - c_{2h\Delta r}^k\ _{L^2(\Omega_2; L_r^2(0, R_\#(\cdot)))}$				
k	$R_h = 1$	$R_h = 2$	$R_h = 3$	Order	k	$R_h = 1$	$R_h = 2$	$R_h = 3$	Order
2	1.72E-04	8.55E-05	4.17E-05	1.04	2	2.01E-12	5.02E-13	1.23E-13	2.04
4	1.33E-04	6.60E-05	3.22E-05	1.03	4	1.69E-12	4.26E-13	1.03E-13	2.04
6	1.09E-04	5.44E-05	2.65E-05	1.03	6	1.48E-12	3.71E-13	9.00E-14	2.04
8	9.85E-05	4.90E-05	2.39E-05	1.03	8	1.41E-12	3.52E-13	8.51E-14	2.05
10	8.94E-05	4.46E-05	2.18E-05	1.03	10	1.34E-12	3.35E-13	8.10E-14	2.05

solver with the optional nonlinear Gauss-Seidel (NGS) decomposition ("2DS-Eta") and the solver only combining the first decoupling with the optional NGS decomposition ("1DS-Eta"). The 2DS-Eta solver is designed to balance solution speed and memory overhead, while 1DS-Eta serves as a baseline to evaluate the impact of Jacobian elimination. We also benchmark these solvers against existing solvers outlined in Appendix C — "GSN-Macro", "GSN-Phi", "GSN-FD" — and the fully coupled solver without any decoupling ("GSN-FC").

The comparison was conducted in the P4D setting with the geometry and battery parameters provided in Appendix B. We considered a simulation time of $T = 20$ s and a uniform time step size of $\tau = 0.1$ s. The grids used for discretization in the radial direction were $\{1 - \frac{1}{2^n}\}_{n=1}^9 \cup \{0, 1\}$, with dimensions in 10^{-6} m. All nonlinear (sub)problems were solved to high accuracy using the Newton's method with an absolute iteration tolerance of $1e-13$. The default line search algorithm in PETSc [53] was employed to ensure robust convergence. The linear system at each Newton step was solved using SuperLU_DIST [54], a distributed-memory sparse direct solver for large sets of linear equations. To enhance computational efficiency, we utilized parallel computing with 252 processes.

We complement the review of existing solvers in Section 1 with the numerical results presented in Table 3. While the GSN-FD solver is attractive due to its simplicity, it proves inefficient in terms of speed and robustness due to the strong coupling and nonlinearity of the system. Moreover, the comparison between the GSN-Phi and GSN-Macro solvers indicates that a higher degree of coupling does not necessarily result in increased efficiency. The superior speed performance of the GSN-FC solver explains its adoption in some software that advertise fast solutions. However, it quickly reaches memory limitations as the problem size increases.

Numerical results demonstrate that the newly proposed solver 2DS-FC significantly outperforms its competitors, nearly doubling the speed of the fastest existing solver. Additionally, its maximum memory usage remains effectively bounded, similar to the GSN-Macro solver. Thanks to the novel NGS decomposition, the number of outer iterations is halved in the 1DS-Eta and 2DS-Eta solvers, with the reduction being contingent on a better understanding of the problem's physics and the strength of coupling between the governing equations. It is worth noting that Jacobian elimination plays a critical role in the 2DS-Eta, accelerating the 1DS-Eta by reducing the matrix order. This reduction is particularly valuable when using tetrahedral meshes,

where the number of elements can be approximately five times the number of nodes. Therefore, the 2DS-Eta solver appears to be a good choice when there are stricter memory constraints.

5. Conclusions

In this paper, we first present an error analysis of the backward Euler finite element discretization for the DFN model of lithium-ion cells. Building on the multiscale projection from [18], we establish the optimal convergence rates in N -dimensions ($1 \leq N \leq 3$) for the first time.

We then propose a novel and highly efficient solver that reduces computational complexity through two decoupling procedures. The first decoupling reduces the dimension from $N + 1$ to N via local inversion, while the second reduces the order of Jacobian, exploiting the Jacobian's reducibility. To further enhance the balance between speed and memory usage, we introduce an optional nonlinear Gauss-Seidel decomposition, which adapts to the problem's physics and the extent of coupling between variables.

Numerical experiments with real battery parameters validate our theoretical results and demonstrate the exceptional performance of the proposed solver. A comprehensive comparison shows that the 2DS solver is the fastest among existing solvers and exhibits robust performance, being largely insensitive to finer microscopic discretization. Additionally, it can be easily combined with other nonlinear Gauss-Seidel decompositions for further optimization.

The DFN model is the most widely used physics-based model for lithium-ion cells and a cornerstone of battery multi-physics modeling. Our theoretical analysis ensures the reliability of the numerical scheme, while the efficient solver can be applied in fields requiring high accuracy and fast computations, such as real-time battery monitoring, estimation, or battery design optimization.

Appendix A. Function spaces and notations

Let $H^m(\Omega)$ ($m \in \mathbb{N}_0$) denote the Sobolev spaces $W^{m,2}(\Omega)$ defined on a generic bounded domain Ω with the norm $\|\cdot\|_{m,\Omega} = \|\cdot\|_{W^{m,2}(\Omega)}$. We also denote the subspace of $H^1(\Omega)$, consisting of functions whose integral is zero, by

$$H_*^1(\Omega) := \left\{ v \in H^1(\Omega) : \int_{\Omega} v \, dx = 0 \right\}.$$

Table 3: Performance Comparison Table

(a) Parallel running time (hours)

#Nodes	#Elems	GSN-FD	GSN-Phi	GSN-Macro	GSN-FC	1DS-Eta	2DS-Eta	2DS-FC
510	2135	0.14	0.07	0.08	0.03	0.06	0.05	0.02
3424	17080	0.81	0.33	0.51	0.23	0.40	0.22	0.10
25007	136640	7.27	2.61	4.34	1.78	2.83	1.76	0.79
190973	1093120	95.67	30.67	56.36	20.79	36.35	17.74	10.11

(b) Total CPU time (hours)

#Nodes	#Elems	GSN-FD	GSN-Phi	GSN-Macro	GSN-FC	1DS-Eta	2DS-Eta	2DS-FC
510	2135	34.84	17.22	34.45	6.99	15.03	12.76	4.39
3424	17080	204.41	81.38	128.11	57.69	99.50	54.17	24.06
25007	136640	1826.68	655.10	1090.04	446.84	712.10	441.89	198.71
190973	1093120	24043.68	7707.35	14162.93	5224.92	9132.94	4457.45	2540.35

(c) Average number of outer iterations

#Nodes	#Elems	GSN-FD	GSN-Phi	GSN-Macro	GSN-FC	1DS-Eta	2DS-Eta	2DS-FC
510	2135	19.06	10.13	9.80	1.00	5.33	5.38	1.00
3424	17080	29.15	10.22	9.87	1.00	4.73	4.73	1.00
25007	136640	34.29	10.09	9.81	1.00	4.64	4.64	1.00
190973	1093120	36.18	9.96	9.72	1.00	4.86	4.94	1.00

(d) Max memory usage (GB)

#Nodes	#Elems	GSN-FD	GSN-Phi	GSN-Macro	GSN-FC	1DS-Eta	2DS-Eta	2DS-FC
510	2135	16.65	16.83	16.68	16.73	17.04	16.97	16.12
3424	17080	23.25	22.98	24.13	30.32	24.93	23.31	23.44
25007	136640	63.25	69.81	79.28	137.85	84.13	69.99	75.92
190973	1093120	390.10	438.00	532.02	985.57	552.79	471.34	532.79

Since multiple domains Ω_n , Ω_s and Ω_p are involved, it is necessary to further define piecewise Sobolev spaces

$$H_{\text{pw}}^m(\Omega_1) = H^m(\Omega_n) \cap H^m(\Omega_s) \cap H^m(\Omega_p)$$

equipped with the norm $\|\cdot\|_{m,\Omega_1} := \|\cdot\|_{m,\Omega_n} + \|\cdot\|_{m,\Omega_s} + \|\cdot\|_{m,\Omega_p}$, and

$$H_{\text{pw}}^m(\Omega_2) = H^m(\Omega_n) \cap H^m(\Omega_p)$$

with $\|\cdot\|_{m,\Omega_2} := \|\cdot\|_{m,\Omega_n} + \|\cdot\|_{m,\Omega_p}$.

The natural space for radial solutions with radial coordinate r is $L_r^2(0, R)$, consisting of measurable functions v defined on $(0, R)$ such that vr is L^2 -integrable. It is obvious that $L_r^2(0, R)$ is a Hilbert space and can be endowed with the norm

$$\|v\|_{L_r^2(0,R)} = \left(\int_0^R |v(r)|^2 r^2 dr \right)^{\frac{1}{2}}.$$

We also denote by $H_r^m(0, R)$ ($m \in \mathbb{N}_0$) the Hilbert spaces of measurable functions v , whose distribution derivatives belong to $L_r^2(0, R)$ up to order m , with the norm

$$\|v\|_{H_r^m(0,R)} = \left(\sum_{k=0}^m \left\| \frac{d^k v}{dr^k} \right\|_{L_r^2(0,R)}^2 \right)^{\frac{1}{2}}. \quad (\text{A.1})$$

For functions in $H_r^1(0, R)$, we have the following critical trace estimation in [23]:

Proposition Appendix A.1. *There exist an arbitrarily small number ϵ and a positive (possibly large) constant $C(\epsilon)$, such that for $u \in H_r^1(0, R)$,*

$$|u(R)| \leq \epsilon \left\| \frac{\partial u}{\partial r} \right\|_{L_r^2(0,R)} + C(\epsilon) \|u\|_{L_r^2(0,R)}.$$

Let X be a Banach space. Vector-valued Lebesgue spaces $L^p(\Omega; X)$, $1 \leq p \leq \infty$, and Sobolev spaces $H^m(\Omega; X)$, $m \in \mathbb{N}_0$, for a generic domain Ω are introduced. It is convenient for c_2 with Ω_2 and R_s in Section 1 to define

$$H^p(\Omega_2; H_r^q(0, R_s(\cdot))) := H^p(\Omega_n; H_r^q(0, R_n)) \cap H^p(\Omega_p; H_r^q(0, R_p)), \quad p, q \in \mathbb{N}_0,$$

with the norm $\|\cdot\|_{p,\Omega_2;q,r} = \|\cdot\|_{H^p(\Omega_n; H_r^q(0, R_n))} + \|\cdot\|_{H^p(\Omega_p; H_r^q(0, R_p))}$. Besides, for time-dependent variables with $\Omega = [0, T]$, notations $(H^m(0, T; X), \|\cdot\|_{m;X})$ are used, and for a partition of the interval $[0, T]$, $0 = t_0 < t_1 < \dots < t_M = T$, we define $\|\cdot\|_{0,k;X} := \left(\int_{t_{k-1}}^{t_k} \|\cdot\|_X^2 dt \right)^{\frac{1}{2}}$, $k = 1, 2, \dots, M$.

Appendix B. Numerical error and order in 3D

In this example, we set $\Omega_n = [0, 50] \times [0, 111.8] \times [0, 111.8]$, $\Omega_s = [50, 75.4] \times [0, 111.8] \times [0, 111.8]$, and $\Omega_p = [75.4, 111.8] \times [0, 111.8] \times [0, 111.8]$ (all dimensions in 10^{-6}m). The boundary Γ is defined as $\Gamma_n \cup \Gamma_p$, where $\Gamma_n = \{0\} \times [0, 111.8] \times [0, 111.8]$ and $\Gamma_p = \{111.8\} \times [0, 111.8] \times [0, 111.8]$. A 5C (30A) discharge rate is applied, using parameters from [3].

The initial spatial mesh is shown by Figure B.4 and the initial radial grid is uniform with the grid size $\Delta r = 1.25 \times 10^{-7}\text{m}$. The finite element solution in an extremely fine mesh ($R_h = 5$ and $R_{\Delta r} = 5$) with a sufficiently small step size $\tau_{\text{ref}} = 0.15625\text{s}$ is taken as the reference solution.

Fixing $R_h = 5$, $R_{\Delta r} = 5$ and refining the initial time step size twice, the convergence error and order of all numerical solutions with respect to τ at $T = 2.5\text{ s}$ are presented in Table B.4. Fixing $R_{\Delta r} = 5$, $\tau = \tau_{\text{ref}}$ and refining the initial spatial mesh twice, the convergence error and order with respect to h at $t_k = k\tau$ are presented in Table B.5. We can clearly see the convergence rates $\mathcal{O}(\tau)$ and $\mathcal{O}(h)$, which agree with our analysis.

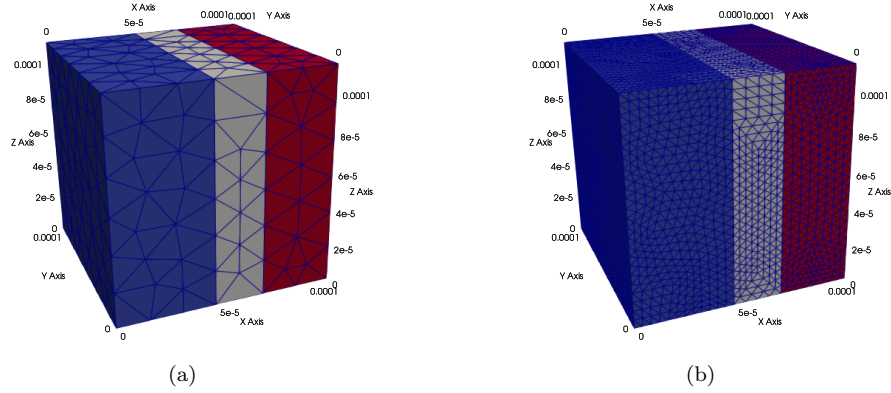


Figure B.4: Spatial meshes for convergence verification. (a) Initial coarse mesh ($R_h = 0$). (b) Uniformly refined mesh ($R_h = 2$).

Appendix C. Decomposition solvers in the literature

Here, we provide a comprehensive list of all decomposition solvers available in the literature, to the best of our knowledge, whose performance is compared in Subsection 4.2.

Table B.4: Error and convergence order for τ .

$t_k = 2.5[s]$	$R_\tau = 0$	$R_\tau = 1$	$R_\tau = 2$	Order
$\ c_1(\cdot, t_k) - c_{1h}^k\ _{H^1}$	1.08E-01	5.17E-02	2.32E-02	1.16
$\ \bar{c}_2(\cdot, t_k) - \bar{c}_{2h}^k\ _{L^2}$	3.04E-01	1.40E-01	6.07E-02	1.21
$\ \phi_1(\cdot, t_k) - \phi_{1h}^k\ _{H^1}$	3.28E-06	1.44E-06	6.46E-07	1.15
$\ \phi_2(\cdot, t_k) - \phi_{2h}^k\ _{H^1}$	3.22E-08	2.92E-09	1.32E-09	1.15

Table B.5: Error and convergence order for h .

(a) $\ \phi_1(\cdot, t_k) - \phi_{1h}^k\ _{H^1(\Omega)}$					(b) $\ \phi_2(\cdot, t_k) - \phi_{2h}^k\ _{H^1(\Omega_2)}$				
k	$R_h = 0$	$R_h = 1$	$R_h = 2$	Order	k	$R_h = 0$	$R_h = 1$	$R_h = 2$	Order
1	4.48E-06	2.51E-06	1.29E-06	0.96	1	7.40E-07	3.75E-07	1.85E-07	1.02
16	9.48E-06	4.85E-06	2.39E-06	1.02	16	7.40E-07	3.75E-07	1.85E-07	1.02
32	1.20E-05	6.06E-06	2.98E-06	1.02	32	7.40E-07	3.75E-07	1.85E-07	1.02
64	1.50E-05	7.57E-06	3.72E-06	1.02	64	7.40E-07	3.75E-07	1.85E-07	1.02
(c) $\ c_1(\cdot, t_k) - c_{1h}^k\ _{H^1(\Omega)}$					(d) $\ \bar{c}_2(\cdot, t_k) - \bar{c}_{2h}^k\ _{L^2(\Omega_2)}$				
k	$R_h = 0$	$R_h = 1$	$R_h = 2$	Order	k	$R_h = 0$	$R_h = 1$	$R_h = 2$	Order
1	7.29E-02	4.94E-02	2.70E-02	0.87	1	5.29E-01	2.93E-01	1.49E-01	0.97
16	2.46E-01	1.27E-01	6.25E-02	1.02	16	1.32E+00	6.76E-01	3.33E-01	1.02
32	3.26E-01	1.66E-01	8.16E-02	1.02	32	1.51E+00	7.66E-01	3.77E-01	1.02
64	4.26E-01	2.16E-01	1.06E-01	1.02	64	1.56E+00	7.90E-01	3.88E-01	1.02

Let $(\phi_{1h}^{k-1}, \phi_{2h}^{k-1}, c_{1h}^{k-1}, c_{2h\Delta r}^{k-1})$ be the fully discrete solution of the $(k-1)$ -th time step. We focus on solving for the solution at the k -th time step, $(\phi_{1h}^k, \phi_{2h}^k, c_{1h}^k, c_{2h\Delta r}^k)$. All solvers considered in this study follow the same initialization and convergence check procedures as described below:

(Initialization): Set the initial guess $X^0 := (c_{1h}^{k,0}, \phi_{1h}^{k,0}, \phi_{2h}^{k,0}, c_{2h\Delta r}^{k,0})$, typically as

$$\phi_{1h}^{k,0} = \phi_{1h}^{k-1}, \phi_{2h}^{k,0} = \phi_{2h}^{k-1}, c_{1h}^{k,0} = c_{1h}^{k-1}, c_{2h\Delta r}^{k,0} = c_{2h\Delta r}^{k-1}.$$

Define the auxiliary quantities

$$\bar{c}_{2h}^{k,0} = c_{2h\Delta r}^{k,0}(\cdot, R_s(\cdot)), U_h^{k,0} = \sum_{m \in \{n,p\}} U_m(\bar{c}_{2h}^{k,0}) \mathbf{1}_{\Omega_m}, \eta_h^{k,0} = \phi_{2h}^{k,0} - \phi_{1h}^{k,0} - U_h^{k,0}.$$

Let $rtol$ be the relative tolerance and set the iteration index $n = 1$.

(Convergence Check): $X^n := (c_{1h}^{k,n}, \phi_{1h}^{k,n}, \phi_{2h}^{k,n}, c_{2h\Delta r}^{k,n})$. If $\left\| \frac{X^n - X^{n-1}}{X^{n-1}} \right\|_{l^\infty} < rtol$, then the iteration is terminated, and we set $\phi_{1h}^k = \phi_{1h}^{k,n}$, $\phi_{2h}^k = \phi_{2h}^{k,n}$, $c_{1h}^k = c_{1h}^{k,n}$, $c_{2h\Delta r}^k = c_{2h\Delta r}^{k,n}$. Otherwise, set $n = n + 1$, update the auxiliary quantities, and continue the iteration.

Appendix C.1. Macroscale-coupled solver [46]

Step 1 (Subproblem (c_1, ϕ_1, ϕ_2)): Find $c_{1h}^{k,n} \in V_h^{(1)}(\bar{\Omega})$, $\phi_{1h}^{k,n} \in W_h(\bar{\Omega})$ and $\phi_{2h}^{k,n} \in V_h^{(1)}(\bar{\Omega}_2)$, such that for all $v_{1h} \in V_h^{(1)}(\bar{\Omega})$, $w_h \in W_h(\bar{\Omega})$ and $v_{2h} \in V_h^{(1)}(\bar{\Omega}_2)$,

$$\begin{aligned} \int_{\Omega} \varepsilon_1 \frac{c_{1h}^{k,n} - c_{1h}^{k-1}}{\tau} v_{1h} \, dx + \int_{\Omega} k_1 \nabla c_{1h}^{k,n} \cdot \nabla v_{1h} \, dx \\ - \int_{\Omega_2} \left(\sum_{m \in \{n,p\}} a_1 J_m(c_{1h}^{k,n}, \bar{c}_{2h}^{k,n-1}, \tilde{\eta}_h^{k,n}) \mathbf{1}_{\Omega_m} \right) v_{1h} \, dx = 0, \quad (C.1) \end{aligned}$$

$$\begin{aligned} \int_{\Omega} \kappa_{1h}^{k,n} \nabla \phi_{1h}^{k,n} \cdot \nabla w_h \, dx - \int_{\Omega} \kappa_{2h}^{k,n} \nabla f(c_{1h}^{k,n}) \cdot \nabla w_h \, dx \\ - \int_{\Omega_2} \left(\sum_{m \in \{n,p\}} a_2 J_m(c_{1h}^{k,n}, \bar{c}_{2h}^{k,n-1}, \tilde{\eta}_h^{k,n}) \mathbf{1}_{\Omega_m} \right) w_h \, dx = 0, \quad (C.2) \end{aligned}$$

$$\int_{\Omega_2} \sigma \nabla \phi_{2h}^{k,n} \cdot \nabla v_{2h} \, dx + \int_{\Omega_2} \left(\sum_{m \in \{n,p\}} a_2 J_m \left(c_{1h}^{k,n}, \bar{c}_{2h}^{k,n-1}, \tilde{\eta}_h^{k,n} \right) \mathbf{1}_{\Omega_m} \right) v_{2h} \, dx + \int_{\Gamma} I^k v_{2h} \, dx = 0, \quad (C.3)$$

where $\kappa_{ih}^{k,n} = \sum_{m \in \{n,s,p\}} \kappa_{im} \left(c_{1h}^{k,n} \right) \mathbf{1}_{\Omega_m}$, $i = 1, 2$ and $\tilde{\eta}_h^{k,n} = \phi_{2h}^{k,n} - \phi_{1h}^{k,n} - U_h^{k,m-1}$.

Step 2 (Subproblem c_2): Find $c_{2h\Delta r}^{k,n} \in V_{h\Delta r}(\bar{\Omega}_{2r})$, such that for all $v_{h\Delta r} \in V_{h\Delta r}(\bar{\Omega}_{2r})$,

$$\int_{\Omega_2} \int_0^{R_s(x)} \frac{c_{2h\Delta r}^{k,n} - c_{2h\Delta r}^{k-1}}{\tau} v_{h\Delta r} r^2 \, dr \, dx + \int_{\Omega_2} \int_0^{R_s(x)} k_2 \frac{\partial c_{2h\Delta r}^{k,n}}{\partial r} \frac{\partial v_{h\Delta r}}{\partial r} r^2 \, dr \, dx + \int_{\Omega_2} \left(\sum_{m \in \{n,p\}} \frac{R_s^2}{F} J_m \left(c_{1h}^{k,n}, \bar{c}_{2h}^{k,n}, \eta_h^{k,n} \right) \mathbf{1}_{\Omega_m} \right) v_{h\Delta r}(x, R_s(x)) \, dx = 0, \quad (C.4)$$

where $\eta_h^{k,n} = \phi_{2h}^{k,n} - \phi_{1h}^{k,n} - U_h^{k,n}$, and $U_h^{k,n} = \sum_{m \in \{n,p\}} U_m(\bar{c}_{2h}^{k,n}) \mathbf{1}_{\Omega_m}$.

Appendix C.2. Potential-coupled solver [13]

Step 1 (Subproblem c_1): Find $c_{1h}^{k,n} \in V_h^{(1)}(\bar{\Omega})$, such that for all $v_h \in V_h^{(1)}(\bar{\Omega})$,

$$\int_{\Omega} \varepsilon_1 \frac{c_{1h}^{k,n} - c_{1h}^{k-1}}{\tau} v_h \, dx + \int_{\Omega} k_1 \nabla c_{1h}^{k,n} \cdot \nabla v_h \, dx - \int_{\Omega_2} \left(\sum_{m \in \{n,p\}} a_1 J_m \left(c_{1h}^{k,n}, \bar{c}_{2h}^{k,n-1}, \eta_h^{k,n-1} \right) \mathbf{1}_{\Omega_m} \right) v_h \, dx = 0. \quad (C.5)$$

Step 2 (Subproblem (ϕ_1, ϕ_2)): Find $\phi_{1h}^{k,n} \in W_h(\bar{\Omega})$, $\phi_{2h}^{k,n} \in V_h^{(1)}(\bar{\Omega}_2)$, such that for all $w_h \in W_h(\bar{\Omega})$, $v_h \in V_h^{(1)}(\bar{\Omega}_2)$,

$$\int_{\Omega} \kappa_{1h}^{k,n} \nabla \phi_{1h}^{k,n} \cdot \nabla w_h \, dx - \int_{\Omega} \kappa_{2h}^{k,n} \nabla f \left(c_{1h}^{k,n} \right) \cdot \nabla w_h \, dx - \int_{\Omega_2} \left(\sum_{m \in \{n,p\}} a_2 J_m \left(c_{1h}^{k,n}, \bar{c}_{2h}^{k,n-1}, \tilde{\eta}_h^{k,n} \right) \mathbf{1}_{\Omega_m} \right) w_h \, dx = 0, \quad (C.6)$$

$$\int_{\Omega_2} \sigma \nabla \phi_{2h}^{k,n} \cdot \nabla v_h \, dx + \int_{\Omega_2} \left(\sum_{m \in \{n,p\}} a_2 J_m \left(c_{1h}^{k,n}, \bar{c}_{2h}^{k,n-1}, \tilde{\eta}_h^{k,n} \right) \mathbf{1}_{\Omega_m} \right) v_h \, dx + \int_{\Gamma} I^k v_h \, dx = 0, \quad (C.7)$$

where $\kappa_{ih}^{k,n} = \sum_{m \in \{n,s,p\}} \kappa_{im} \left(c_{1h}^{k,n} \right) \mathbf{1}_{\Omega_m}$, $i = 1, 2$, $\tilde{\eta}_h^{k,n} = \phi_{2h}^{k,n} - \phi_{1h}^{k,n} - U_h^{k,n-1}$.

Step 3 (Subproblem c_2): Find $c_{2h\Delta r}^{k,n} \in V_{h\Delta r}(\bar{\Omega}_{2r})$, such that for all $v_{h\Delta r} \in V_{h\Delta r}(\bar{\Omega}_{2r})$,

$$\int_{\Omega_2} \int_0^{R_s(x)} \frac{c_{2h\Delta r}^{k,n} - c_{2h\Delta r}^{k-1}}{\tau} v_{h\Delta r} r^2 \, dr \, dx + \int_{\Omega_2} \int_0^{R_s(x)} k_2 \frac{\partial c_{2h\Delta r}^{k,n}}{\partial r} \frac{\partial v_{h\Delta r}}{\partial r} r^2 \, dr \, dx + \int_{\Omega_2} \left(\sum_{m \in \{n,p\}} \frac{R_s^2}{F} J_m \left(c_{1h}^{k,n}, \bar{c}_{2h}^{k,n}, \eta_h^{k,n} \right) \mathbf{1}_{\Omega_m} \right) v_{h\Delta r}(x, R_s(x)) \, dx = 0, \quad (C.8)$$

where $\eta_h^{k,n} = \phi_{2h}^{k,n} - \phi_{1h}^{k,n} - U_h^{k,n}$, and $U_h^{k,n} = \sum_{m \in \{n,p\}} U_m(\bar{c}_{2h}^{k,n}) \mathbf{1}_{\Omega_m}$.

Appendix C.3. Fully decoupled solver [42]

Step 1 (Subproblem c_2): Find $c_{2h\Delta r}^{k,n} \in V_{h\Delta r}(\bar{\Omega}_{2r})$, such that for all $v_{h\Delta r} \in V_{h\Delta r}(\bar{\Omega}_{2r})$,

$$\int_{\Omega_2} \int_0^{R_s(x)} \frac{c_{2h\Delta r}^{k,n} - c_{2h\Delta r}^{k-1}}{\tau} v_{h\Delta r} r^2 \, dr \, dx + \int_{\Omega_2} \int_0^{R_s(x)} k_2 \frac{\partial c_{2h\Delta r}^{k,n}}{\partial r} \frac{\partial v_{h\Delta r}}{\partial r} r^2 \, dr \, dx + \int_{\Omega_2} \left(\sum_{m \in \{n,p\}} \frac{R_s^2}{F} J_m \left(c_{1h}^{k,n-1}, \bar{c}_{2h}^{k,n}, \tilde{\eta}_h^{k,n} \right) \mathbf{1}_{\Omega_m} \right) v_{h\Delta r}(x, R_s(x)) \, dx = 0,$$

where $\tilde{\eta}_h^{k,n} = \phi_{2h}^{k,n-1} - \phi_{1h}^{k,n-1} - U_h^{k,n}$, and $U_h^{k,n} = \sum_{m \in \{n,p\}} U_m(\bar{c}_{2h}^{k,n}) \mathbf{1}_{\Omega_m}$.

Step 2 (Subproblem ϕ_2): Find $\phi_{2h}^{k,n} \in V_h^{(1)}(\bar{\Omega}_2)$, such that for all $v_h \in V_h^{(1)}(\bar{\Omega}_2)$,

$$\int_{\Omega_2} \sigma \nabla \phi_{2h}^{k,n} \cdot \nabla v_h \, dx + \int_{\Omega_2} \left(\sum_{m \in \{n,p\}} a_2 J_m \left(c_{1h}^{k,n}, \bar{c}_{2h}^{k,n-1}, \tilde{\eta}_h^{k,n} \right) \mathbf{1}_{\Omega_m} \right) v_h \, dx + \int_{\Gamma} I^k v_h \, dx = 0,$$

where $\tilde{\eta}_h^{k,n} = \phi_{2h}^{k,n} - \phi_{1h}^{k,n-1} - U_h^{k,n}$.

Step 3 (Subproblem ϕ_1): Find $\phi_{1h}^{k,n} \in V_h^{(1)}(\bar{\Omega})$, such that for all $w_h \in V_h^{(1)}(\bar{\Omega})$,

$$\begin{aligned} \int_{\Omega} \kappa_{1h}^{k,n-1} \nabla \phi_{1h}^{k,n} \cdot \nabla w_h \, dx - \int_{\Omega} \kappa_{2h}^{k,n-1} \nabla f(c_{1h}^{k,n-1}) \cdot \nabla w_h \, dx \\ - \int_{\Omega_2} \left(\sum_{m \in \{n,p\}} a_2 J_m(c_{1h}^{k,n-1}, c_{2h}^{k,n}, \eta_h^{k,n}) \mathbf{1}_{\Omega_m} \right) w_h \, dx = 0, \quad (\text{C.9}) \end{aligned}$$

where $\eta_h^{k,n} = \phi_{2h}^{k,n} - \phi_{1h}^{k,n} - U_h^{k,n}$.

Step 4 (Subproblem c_1): Find $c_{1h}^{k,n} \in V_h^{(1)}(\bar{\Omega})$, such that for all $v_h \in V_h^{(1)}(\bar{\Omega})$,

$$\begin{aligned} \int_{\Omega} \varepsilon_1 \frac{c_{1h}^{k,n} - c_{1h}^{k-1}}{\tau} v_h \, dx + \int_{\Omega} k_1 \nabla c_{1h}^{k,n} \cdot \nabla v_h \, dx \\ - \int_{\Omega_2} \left(\sum_{m \in \{n,p\}} a_1 J_m(c_{1h}^{k,n}, c_{2h}^{k,n}, \eta_h^{k,n}) \mathbf{1}_{\Omega_m} \right) v_h \, dx = 0. \end{aligned}$$

References

- [1] M. Doyle, T. F. Fuller, J. Newman, Modeling of galvanostatic charge and discharge of the lithium/polymer/insertion cell, *Journal of The Electrochemical Society* 140 (1993) 1526–1533. doi:10.1149/1.2221597.
- [2] T. F. Fuller, M. Doyle, J. Newman, Simulation and optimization of the dual lithium ion insertion cell, *Journal of The Electrochemical Society* 141 (1994) 1–10. URL: <https://iopscience.iop.org/article/10.1149/1.2054684>. doi:10.1149/1.2054684.
- [3] K. Smith, C.-Y. Wang, Solid-state diffusion limitations on pulse operation of a lithium ion cell for hybrid electric vehicles, *Journal of Power Sources* 161 (2006) 628–639. doi:10.1016/j.jpowsour.2006.03.050.
- [4] V. Ramadesigan, P. W. C. Northrop, S. De, S. Santhanagopalan, R. D. Braatz, V. R. Subramanian, Modeling and simulation of lithium-ion batteries from a systems engineering perspective, *Journal of The Electrochemical Society* 159 (2012) R31. URL: <https://iopscience.iop.org/article/10.1149/2.018203jes/meta>. doi:10.1149/2.018203jes.

- [5] S. Shi, J. Gao, Y. Liu, Y. Zhao, Q. Wu, W. Ju, C. Ouyang, R. Xiao, Multi-scale computation methods: Their applications in lithium-ion battery research and development, *Chinese Physics B* 25 (2015) 018212.
- [6] G. L. Plett, *Battery Management Systems*, volume 1, Artech House, Boston, 2015.
- [7] T. Telmasre, N. Goswami, A. Concepción, S. Kolluri, M. Pathak, G. Morrison, V. R. Subramanian, Impedance response simulation strategies for lithium-ion battery models, *Current Opinion in Electrochemistry* 36 (2022) 101140. URL: <https://linkinghub.elsevier.com/retrieve/pii/S2451910322002058>. doi:10.1016/j.coelec.2022.101140.
- [8] L. Wu, Z. Lyu, Z. Huang, C. Zhang, C. Wei, Physics-based battery SOC estimation methods: Recent advances and future perspectives, *Journal of Energy Chemistry* 89 (2024) 27–40. URL: <https://linkinghub.elsevier.com/retrieve/pii/S209549562300565X>. doi:10.1016/j.jechem.2023.09.045.
- [9] S. Golmon, K. Maute, M. L. Dunn, Multiscale design optimization of lithium ion batteries using adjoint sensitivity analysis, *International Journal for Numerical Methods in Engineering* 92 (2012) 475–494. URL: <https://onlinelibrary.wiley.com/doi/abs/10.1002/nme.4347>. doi:<https://doi.org/10.1002/nme.4347>.
- [10] K. S. Hariharan, P. Tagade, S. Ramachandran, *Mathematical Modeling of Lithium Batteries*, Springer International Publishing, Cham, 2018. URL: <http://link.springer.com/10.1007/978-3-319-03527-7>. doi:10.1007/978-3-319-03527-7.
- [11] Z. Chen, D. L. Danilov, R.-A. Eichel, P. H. L. Notten, Porous Electrode Modeling and its Applications to Li-Ion Batteries, *Advanced Energy Materials* 12 (2022) 2201506. URL: <https://onlinelibrary.wiley.com/doi/abs/10.1002/aenm.202201506>. doi:10.1002/aenm.202201506.
- [12] F. B. Planella, W. Ai, A. M. Boyce, A. Ghosh, I. Korotkin, S. Sahu, V. Sulzer, R. Timms, T. G. Tranter, M. Zyskin, S. J. Cooper, J. S. Edge, J. M. Foster, M. Marinescu, B. Wu, G. Richardson, A continuum of

- physics-based lithium-ion battery models reviewed, *Progress in Energy* 4 (2022) 042003. URL: <https://dx.doi.org/10.1088/2516-1083/ac7d31>. doi:10.1088/2516-1083/ac7d31.
- [13] R. Bermejo, P. G. d. Sastre, An implicit-explicit Runge-Kutta-Chebyshev finite element method for the nonlinear Lithium-ion battery equations, *Applied Mathematics and Computation* 361 (2019) 398–420. doi:10.1016/j.amc.2019.05.011.
 - [14] F. Ciucci, W. Lai, Derivation of micro/macro lithium battery models from homogenization, *Transport in Porous Media* 88 (2011) 249–270. doi:10.1007/s11242-011-9738-5.
 - [15] H. Arunachalam, S. Onori, I. Battiato, On veracity of macroscopic Lithium-ion battery models, *Journal of The Electrochemical Society* 162 (2015) A1940. URL: <https://iopscience.iop.org/article/10.1149/2.0771509jes/meta>. doi:10.1149/2.0771509jes.
 - [16] R. Timms, S. G. Marquis, V. Sulzer, C. P. Please, S. J. Chapman, Asymptotic reduction of a Lithium-ion pouch cell model, *SIAM Journal on Applied Mathematics* 81 (2021) 765–788. doi:10.1137/20M1336898.
 - [17] G. W. Richardson, J. M. Foster, R. Ranom, C. P. Please, A. M. Ramos, Charge transport modelling of Lithium-ion batteries, *European Journal of Applied Mathematics* 33 (2022) 983–1031. doi:10.1017/S0956792521000292.
 - [18] S. Xu, L. Cao, Optimal convergence in finite element semi-discrete error analysis of the Doyle-Fuller-Newman model beyond 1D with a novel projection operator, *IMA Journal of Numerical Analysis* (2025). URL: <https://arxiv.org/abs/2411.10758>. doi:10.1093/imanum/draf065, to appear.
 - [19] A. M. Ramos, On the well-posedness of a mathematical model for lithium-ion batteries, *Applied Mathematical Modelling* 40 (2016) 115–125. URL: <https://linkinghub.elsevier.com/retrieve/pii/S0307904X15003546>. doi:10.1016/j.apm.2015.05.006.
 - [20] C. Kroener, A mathematical exploration of a PDE system for lithium-ion batteries, Ph.D. thesis, UC Berkeley, 2016.

- [21] J. I. Díaz, D. Gómez-Castro, A. M. Ramos, On the well-posedness of a multiscale mathematical model for Lithium-ion batteries, *Advances in Nonlinear Analysis* 8 (2019) 1132–1157. doi:10.1515/anona-2018-0041.
- [22] L. Cai, R. E. White, Lithium ion cell modeling using orthogonal collocation on finite elements, *Journal of Power Sources* 217 (2012) 248–255. URL: <https://linkinghub.elsevier.com/retrieve/pii/S0378775312010439>. doi:10.1016/j.jpowsour.2012.06.043.
- [23] R. Bermejo, Numerical analysis of a finite element formulation of the P2D model for Lithium-ion cells, *Numerische Mathematik* 149 (2021) 463–505. doi:10.1007/s00211-021-01235-2.
- [24] J. S. Newman, N. P. Balsara, *Electrochemical systems*, fourth edition ed., Wiley, Hoboken, NJ, 2019.
- [25] Z. Mao, R. E. White, A finite-difference method for pseudo-two-dimensional boundary value problems, *Journal of The Electrochemical Society* 141 (1994) 151. URL: <https://iopscience.iop.org/article/10.1149/1.2054675/meta>. doi:10.1149/1.2054675.
- [26] G. S. Nagarajan, J. W. V. Zee, R. M. Spotnitz, A mathematical model for intercalation electrode behavior: I. Effect of particle-size distribution on discharge capacity, *Journal of The Electrochemical Society* 145 (1998) 771. URL: <https://iopscience.iop.org/article/10.1149/1.1838344/meta>. doi:10.1149/1.1838344.
- [27] Y. Zeng, P. Albertus, R. Klein, N. Chaturvedi, A. Kojic, M. Z. Bazant, J. Christensen, Efficient conservative numerical schemes for 1D nonlinear spherical diffusion equations with applications in battery modeling, *Journal of The Electrochemical Society* 160 (2013) A1565–A1571. URL: <https://iopscience.iop.org/article/10.1149/2.102309jes>. doi:10.1149/2.102309jes.
- [28] S. Mazumder, J. Lu, Faster-than-real-time simulation of lithium ion batteries with full spatial and temporal resolution, *International Journal of Electrochemistry* 2013 (2013) 1–10. doi:10.1155/2013/268747.

- [29] P. W. C. Northrop, V. Ramadesigan, S. De, V. R. Subramanian, Coordinate transformation, orthogonal collocation, model reformulation and simulation of electrochemical-thermal behavior of lithium-ion battery stacks, *Journal of The Electrochemical Society* 158 (2011) A1461. URL: <https://iopscience.iop.org/article/10.1149/2.058112jes/meta>. doi:10.1149/2.058112jes.
- [30] P. W. C. Northrop, M. Pathak, D. Rife, S. De, S. Santhanagopalan, V. R. Subramanian, Efficient simulation and model reformulation of two-dimensional electrochemical thermal behavior of lithium-ion batteries, *Journal of The Electrochemical Society* 162 (2015) A940–A951. URL: <https://iopscience.iop.org/article/10.1149/2.0341506jes>. doi:10.1149/2.0341506jes.
- [31] S. Kosch, Y. Zhao, J. Sturm, J. Schuster, G. Mulder, E. Ayerbe, A. Jossen, A computationally efficient multi-scale model for lithium-ion cells, *Journal of The Electrochemical Society* 165 (2018) A2374–A2388. URL: <https://iopscience.iop.org/article/10.1149/2.1241810jes>. doi:10.1149/2.1241810jes.
- [32] K. E. Brenan, S. L. Campbell, L. R. Petzold, *Numerical Solution of Initial-Value Problems in Differential-Algebraic Equations*, Society for Industrial and Applied Mathematics, Philadelphia, 1995. URL: <http://epubs.siam.org/doi/book/10.1137/1.9781611971224>. doi:10.1137/1.9781611971224.
- [33] I. Korotkin, S. Sahu, S. O’Kane, G. Richardson, J. M. Foster, Dandelion v1: An extremely fast solver for the Newman model of lithium-ion battery (dis)charge, *Journal of The Electrochemical Society* 168 (2021) 060544. URL: <http://arxiv.org/abs/2102.06534>. doi:10.1149/1945-7111/ac085f.
- [34] T. Wickramanayake, M. Javadipour, K. Mehran, A Novel Solver for an Electrochemical–Thermal Ageing Model of a Lithium-Ion Battery, *Batteries* 10 (2024) 126. URL: <https://www.mdpi.com/2313-0105/10/4/126>. doi:10.3390/batteries10040126, number: 4 Publisher: Multidisciplinary Digital Publishing Institute.
- [35] R. C. Aylagas, C. Ganuza, R. Parra, M. Yañez, E. Ayerbe, cideMOD: An Open Source Tool for Battery Cell Inhomogeneous Per-

- formance Understanding, Journal of The Electrochemical Society 169 (2022) 090528. URL: <https://dx.doi.org/10.1149/1945-7111/ac91fb>. doi:10.1149/1945-7111/ac91fb, publisher: IOP Publishing.
- [36] W. Ai, Y. Liu, JuBat: A Julia-based framework for battery modelling using finite element method, SoftwareX 27 (2024) 101760. URL: <https://linkinghub.elsevier.com/retrieve/pii/S2352711024001316>. doi:10.1016/j.softx.2024.101760.
- [37] COMSOL Multiphysics® v. 6.3, Battery Design Module User's Guide, COMSOL AB, Stockholm, Sweden, 2024.
- [38] S. Golmon, K. Maute, M. L. Dunn, A design optimization methodology for Li+ batteries, Journal of Power Sources 253 (2014) 239–250. URL: <https://linkinghub.elsevier.com/retrieve/pii/S0378775313019939>. doi:10.1016/j.jpowsour.2013.12.025.
- [39] R. Han, C. Macdonald, B. Wetton, A fast solver for the pseudo-two-dimensional model of lithium-ion batteries, 2021. URL: <http://arxiv.org/abs/2111.09251>, arXiv:2111.09251 [physics].
- [40] X. Yin, D. Zhang, batP2dFoam: An Efficient Segregated Solver for the Pseudo-2-Dimensional (P2D) Model of Li-Ion Batteries, Journal of The Electrochemical Society 170 (2023) 030521. URL: <https://dx.doi.org/10.1149/1945-7111/acbfe4>. doi:10.1149/1945-7111/acbfe4, publisher: IOP Publishing.
- [41] W. Ai, Y. Liu, Improving the convergence rate of Newman's battery model using 2nd order finite element method, Journal of Energy Storage 67 (2023) 107512. URL: <https://linkinghub.elsevier.com/retrieve/pii/S2352152X2300909X>. doi:10.1016/j.est.2023.107512.
- [42] J. Kim, A. Mallarapu, S. Santhanagopalan, J. Newman, A robust numerical treatment of solid-phase diffusion in pseudo two-dimensional lithium-ion battery models, Journal of Power Sources 556 (2023) 232413. URL: <https://linkinghub.elsevier.com/retrieve/pii/S0378775322013908>. doi:10.1016/j.jpowsour.2022.232413.
- [43] V. Thomée, Galerkin Finite Element Methods for Parabolic Problems, Springer, Berlin Heidelberg, 2007.

- [44] J. M. O. a. W. C. Rheinboldt, Iterative Solution of Nonlinear Equations in Several Variables (Classics in Applied Mathematics), SIAM, 1987. URL: <http://gen.lib.rus.ec/book/index.php?md5=cf8fe5541f9d65562f5b058898c63ce5>.
- [45] P. R. Brune, M. G. Knepley, B. F. Smith, X. Tu, Composing Scalable Nonlinear Algebraic Solvers, SIAM Review 57 (2015) 535–565. URL: <http://epubs.siam.org/doi/10.1137/130936725>. doi:10.1137/130936725.
- [46] A. Latz, J. Zausch, Multiscale modeling of lithium ion batteries: Thermal aspects, Beilstein Journal of Nanotechnology 6 (2015) 987–1007. URL: <https://www.beilstein-journals.org/bjnano/articles/6/102>. doi:10.3762/bjnano.6.102.
- [47] J. Wu, V. Srinivasan, J. Xu, C. Y. Wang, Newton-Krylov-Multigrid algorithms for battery simulation, Journal of The Electrochemical Society 149 (2002) A1342. URL: <https://iopscience.iop.org/article/10.1149/1.1505635>. doi:10.1149/1.1505635.
- [48] A. Latz, J. Zausch, Thermodynamic derivation of a Butler–Volmer model for intercalation in Li-ion batteries, Electrochimica Acta 110 (2013) 358–362. URL: <https://www.sciencedirect.com/science/article/pii/S0013468613011493>. doi:10.1016/j.electacta.2013.06.043.
- [49] P. G. Ciarlet, The Finite Element Method for Elliptic Problems, Society for Industrial and Applied Mathematics, Philadelphia, 2002.
- [50] J. Xu, Estimate of the convergence rate of finite element solutions to elliptic equations of second order with discontinuous coefficients, Natural Science Journal of Xiangtan University 1 (1982) 84–88.
- [51] B. S. Kirk, J. W. Peterson, R. H. Stogner, G. F. Carey, libMesh: A C++ Library for Parallel Adaptive Mesh Refinement/Coarsening Simulations, Engineering with Computers 22 (2006) 237–254.
- [52] P. Bochev, R. B. Lehoucq, On the Finite Element Solution of the Pure Neumann Problem, SIAM Review 47 (2005) 50–66. URL: <http://epubs.siam.org/doi/10.1137/S0036144503426074>. doi:10.1137/S0036144503426074.

- [53] S. Balay, S. Abhyankar, M. F. Adams, J. Brown, P. Brune, K. Buschelman, L. Dalcin, A. Dener, V. Eijkhout, W. D. Gropp, D. Karpeyev, D. Kaushik, M. G. Knepley, D. A. May, L. C. McInnes, R. T. Mills, T. Munson, K. Rupp, P. Sanan, B. F. Smith, S. Zampini, H. Zhang, H. Zhang, PETSc Users Manual, Technical Report ANL-95/11 - Revision 3.15, Argonne National Laboratory, 2021. URL: <https://www.mcs.anl.gov/petsc>.
- [54] X. S. Li, J. W. Demmel, SuperLU_DIST: A scalable distributed-memory sparse direct solver for unsymmetric linear systems, ACM Trans. Math. Softw. 29 (2003) 110–140. URL: <https://doi.org/10.1145/779359.779361>. doi:10.1145/779359.779361.